AD-A190 501 STRESS CORROSION OF CERAMIC MATERIALS(U) NATIONAL BUREAU OF STANDARDS GAITHERSBURG MD CERAMICS DIV S W FREIMAN ET AL NOV 87 N00014-86-F-0022 1/1

UNCLASSIFIED F/G 11/2 NL

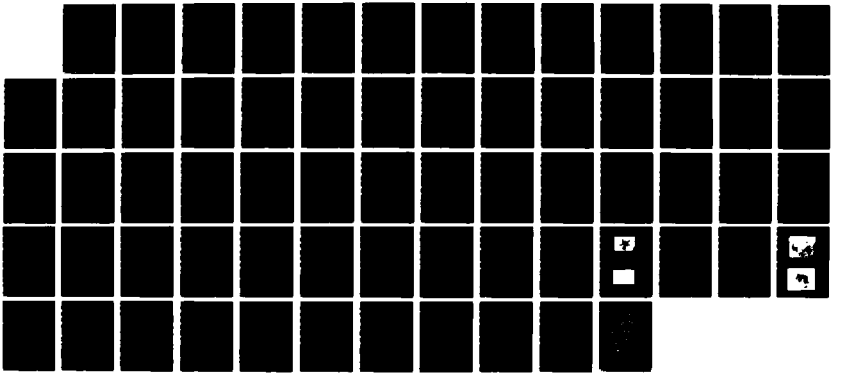

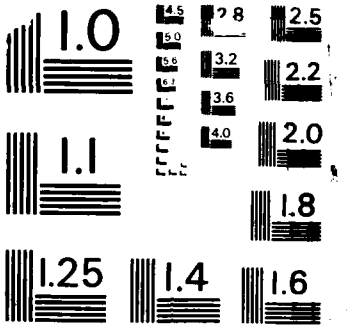

MICROCOPY RESOLUTION TEST CHART

NATIONAL BUREAU OF STANDARDS - 1963 - A

(4)

STRESS CORROSION OF CERAMIC MATERIALS

S. W. Freiman, G. S. White, T. L. Baker, S. M. Wiederhorn, T. D. Coyle, E. R. Fuller, Jr., A. M. Wilson, and L. Chuck

ANNUAL REPORT

October 1, 1985 - September 30, 1986

ONR Contract No. N00014-86-F-0022

for

Office of Naval Research
Code 1131
Arlington, VA 22217

by

Ceramics Division
National Bureau of Standards
Gaithersburg, MD 20899

November, 1987

STRESS CORROSION OF CERAMIC MATERIALS

S. W. Freiman, G. S. White, T. L. Baker, S. M. Wiederhorn, T. D. Coyle,
E. R. Fuller, Jr., A. M. Wilson, and L. Chuck

ANNUAL REPORT

October 1, 1985 - September 30, 1986

ONR Contract No. N00014-86-F-0022

for

Office of Naval Research
Code 1131
Arlington, VA 22217

by

Ceramics Division
National Bureau of Standards
Gaithersburg, MD 20899

November, 1987

Table of Contents

Stress Corrosion of Ceramic Materials

	Page No
Summary.....	1
Environmentally Enhanced Crack Growth In Glass Modeled By Lattice Greens Functions.....	17
Strain Patterns in Gallium Arsenide Wafers: Origins and Effects	42
Mechanical Behavior of Ferroelectric Ceramics.....	56

STRESS CORROSION OF CERAMIC MATERIALS

SUMMARY

The work during fiscal year 1986 can be divided into two distinct areas, namely (1) the fundamental mechanisms involved in environmentally enhanced fracture of single crystals, and (2) fracture behavior of ceramics used in multilayer capacitors. The results of these investigations are summarized as follows:

(1) Environmentally Enhanced Crack Growth

During the past year, effort was directed toward understanding how the ionicity of the chemical bonds in a material determine the environments which enhance fracture in those materials. Previous work has suggested that environments which enhance crack growth in a material are determined by the ionicity of the strained bonds at the crack tip; environments which are polar enhance crack growth in ionic materials such as MgF_2; environments which act as both a Lewis base and acid enhance crack growth in more covalent materials. Last year, we began efforts to evaluate this hypothesis by making crack growth measurements using indentation techniques on a series of small single crystals from the II-VI and III-V columns of the periodic table. The total crack length measured after periods of time in various environments gave an indication of the crystals susceptibility to crack growth in that environment. However, because the shape of the V-K_I curve can not be obtained in this way, mechanisms could not be determined. This year, we have attempted to make crack growth measurements on GaAs single crystals using the DCB technique to delineate the entire crack velocity curve.

The specimens used were commercial, single crystal, undoped wafers grown by the LEC technique and were polished on both sides by the vendor. The

wafers were cut sequentially from the same crystal boule. The crack growth results from all of the specimens were scattered, suggesting that there was a great deal of residual stress present in the material. For instance, crack growth curves had different slopes in different specimens; the apparent K_{Ic} shifted randomly from $=.2$ MPam$^{\frac{1}{2}}$ to $=.5$ MPam$^{\frac{1}{2}}$, and propagating cracks deviated toward or away from microscopic surface flaws in the specimens or deviated to the sides of the specimens.

Because of these problems, quantitative results could not be obtained. However, a number of qualitative conclusions could be drawn, based upon behavior which was repeatedly observed; water and methanol enhanced crack propagation in GaAs; no enhancement of crack growth was observed in heptane, even though it has a high ($\approx$30%) relative humidity; no crack growth was observed in any vapor, i.e. ammonia, water, methanol, or acetonitrile. In addition, crack growth of GaAs in water appeared to exhibit a stress corrosion limit. In water, when the applied load was reduced to drive the crack at velocities below $=10^{-7}$ m/s, no crack extension was detected, and upon raising the load, no further controlled crack growth was ever observed. Methanol did not seem to have a similar stress corrosion limit and, excluding effects due to residual stresses, crack velocities between 10^{-1} and 10^{-9} m/sec were obtained.

Finally, to determine the source of the residual stresses in the specimens, in collaberation with the Center of Electrical and Electronic Engineering, x-ray topograph maps of residual strains in the wafers were correlated with a mapping of indentation crack lengths in the wafers as well as with the strain patterns of adjoining wafers. We found that the specimens were filled with regions of residual strains; these regions ranged in size

from microns to several millimeters square and appeared to be randomly arranged within the wafer. Comparisons between wafers showed that the residual stress patterns were generated during crystal growth and were not alleviated by the thermal anneal the crystal boule underwent before sectioning.

Although the residual stresses in the wafers prevented quantitative determination of the relative strength of different environments in promoting crack growth in GaAs, a preliminary evaluation of the ionicity model for describing environmentally enhanced crack growth can be deduced from the qualitative data. Because GaAs has the same proportion of ionic and covalant contributions to its bonds as does vitreous silica, our model would predict that the same environments should enhance crack growth in both materials. In fact, we find that, although water and methanol do enhance crack growth in both materials, ammonia gas is only effective for vitreous silica. In addition, water and methanol vapor in nitrogen gas and water impurities in heptane appear ineffective at enhancing crack propagation in GaAs although they are effective in silica. Therefore, our results suggest that the model predicting which environments would be effective at enhancing crack growth based simply on the ionicity of the specimen bonds may be over simplified and needs further investigation. Two possible explanations for our observations are that; 1) environmentally enhanced crack growth in GaAs is driven by corrosion processes and, in the vapor phase, the environments cannot remove material quickly enough to maintain crack growth or 2) environments which are effective at enhancing crack growth in GaAs require a high dielectric constant which can only occur in a liquid. However, evaluation of these possibilities as well as quantitative comparisons of environmental effects on fracture

indentation load regime, these data were fitted to a best fit curve of slope = -1/3 as per Equation 1. These curves were then used to calculate the values of critical fracture toughness given in Table 1. The uncertainties in these values were calculated from the uncertainties in the $\sigma P^{1/3}$ values used to fit the curve. In most cases the values of fracture stress at the largest indentation load (usually 100N) were not used in the calculation of toughness because of evidence of extensive lateral cracking occuring at these loads.

The data in Table 1 indicates a significant variation in K_{IC} from one capacitor composition to another. Fractographic evidence (2) suggests that these variations are due to microstructural differences from one composition to another, and more specifically to the degree of crack deflection in the material. Those ceramics exhibiting the largest extent of crack deflection tend to have the highest values of K_{IC} (2). In general, the relaxor compositions (Z5U-3 and PL 802) exhibited fracture toughness values at the lower end of the range for all compositions. Whether these lower toughnesses account for the rumored sensitivity to fracture of these compositions during manufacture, however, cannot be determined at present.

The plots of fracture stress versus indentation load in Figures 1 through 8 indicate that microstructure also plays a part in determining the strength of the capacitor at small flaw sizes. It can be seen that there is a wide variation in the extent of the deviation from the indentation model at small loads. This type of deviation has been ascribed to effects of the microstructure on fracture (3), either through the direct influence of the internal stresses on the driving force for flaw growth, or through an increase in the toughness of the material as the crack size increases from the range of

normal machining induced flaws to that usually associated with classical fracture mechanics procedures.

REFERENCES

1. P. Chantikul, G. R. Anstis, B. R. Lawn, and D. B. Marshall, J. Am. Ceram. Soc., 64, [9], 539-43 (1981)

2. T. L. Baker and S. W. Freiman, Mat. Res. Soc. Symp., 72, 81-90 (1986)

3. S. W. Freiman, to be published in Bull. Am. Ceram. Soc.

Table 1

Compositions and Fracture Toughness Values of Capacitor Ceramics

Designation	Supplier	Major Constituents	K_{IC} ($MPam^{1/2}$)
NPO	AVX	$BaTiO_3$; $NdTiO_3$	1.4^1 (.06)
X7R-1	"	$BaTiO_3$; $Bi_4Ti_3O_7$	1.1^1 (.09) 1.1^2 (.10)
X7R-2	"	$BaTiO_3$ (98.5%)	$.70^1$ (.08)
X7R-2M	"	Modification of X7R-2	$.86^2$ (.08)
X7R-3	"	Modification of X7R-1	1.2^1 (.11) 1.0^2 (.10)
ZSU-1	"	$BaTiO_3$; $CaZrO_3$	$.73^1$ (.07) $.90^2$ (.09)
ZSU-3	"	$Pb(Mg_{.5}Nb_{.5})O_3$	$.87^1$ (.08) $.82^2$ (.14)
T3000	Dupont	$BaTiO_3$	1.0^1 (.09)
XL282	"	$BaTiO_3$ (97%)(X7R)	$.96^1$ (.08)
BL162	"	$BaTiO_3$; Bi containing X7R	1.2^1 (.10)
BL172HD	"	$BaTiO_3$; Bi containing (X7R)	1.5^1 (.23)
XL802	"	$BaTiO_3$; Pb and Zr containing (Z5U)	$.99^1$ (.08)
PL802	"	$PbTiO_3$; $Pb(Mg_{.5},W_{.5})O_3$	$.95^1$ (.04)

( ) Standard deviation based on fit of $\sigma P^{1/3}$

[1] Measured at 22°C in silicone oil
[2] Measured at 3°C in fluorinert

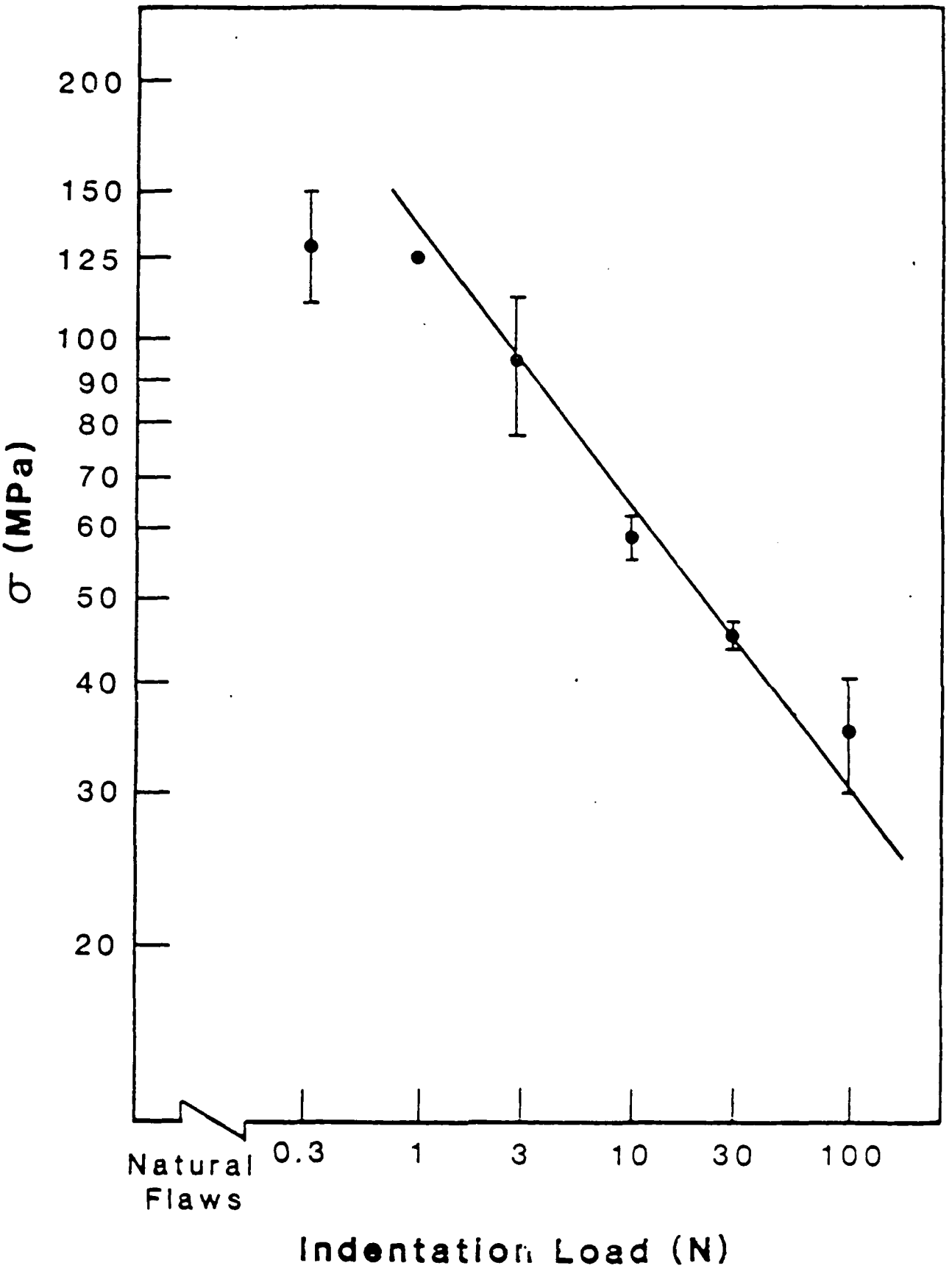

Figure 1 Fracture stress-indentation load plot for X7R-1 (AVX) ceramic.

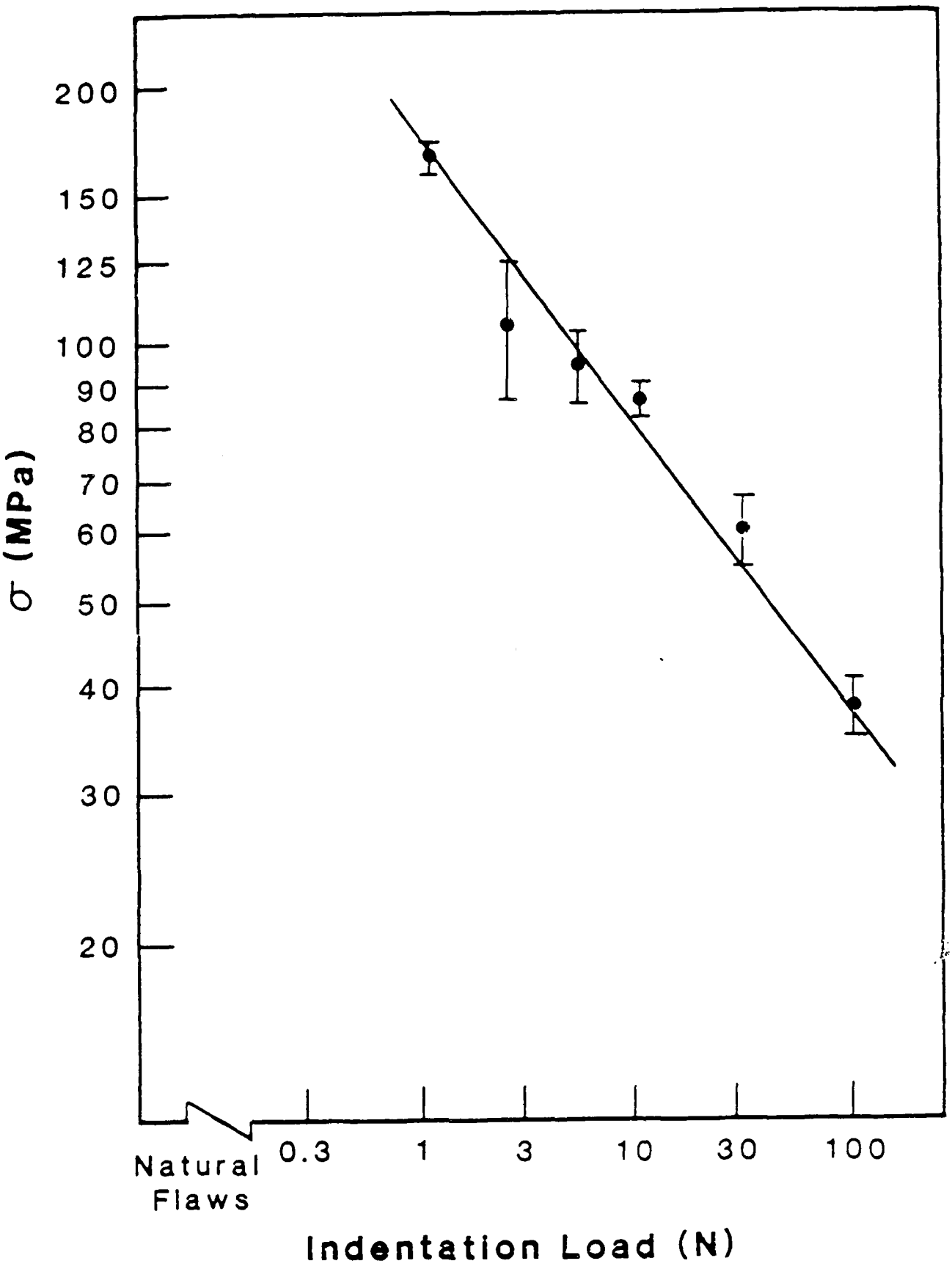

Figure 2 Fracture stress-indentation load plot for X7R-3 (AVX) ceramic.

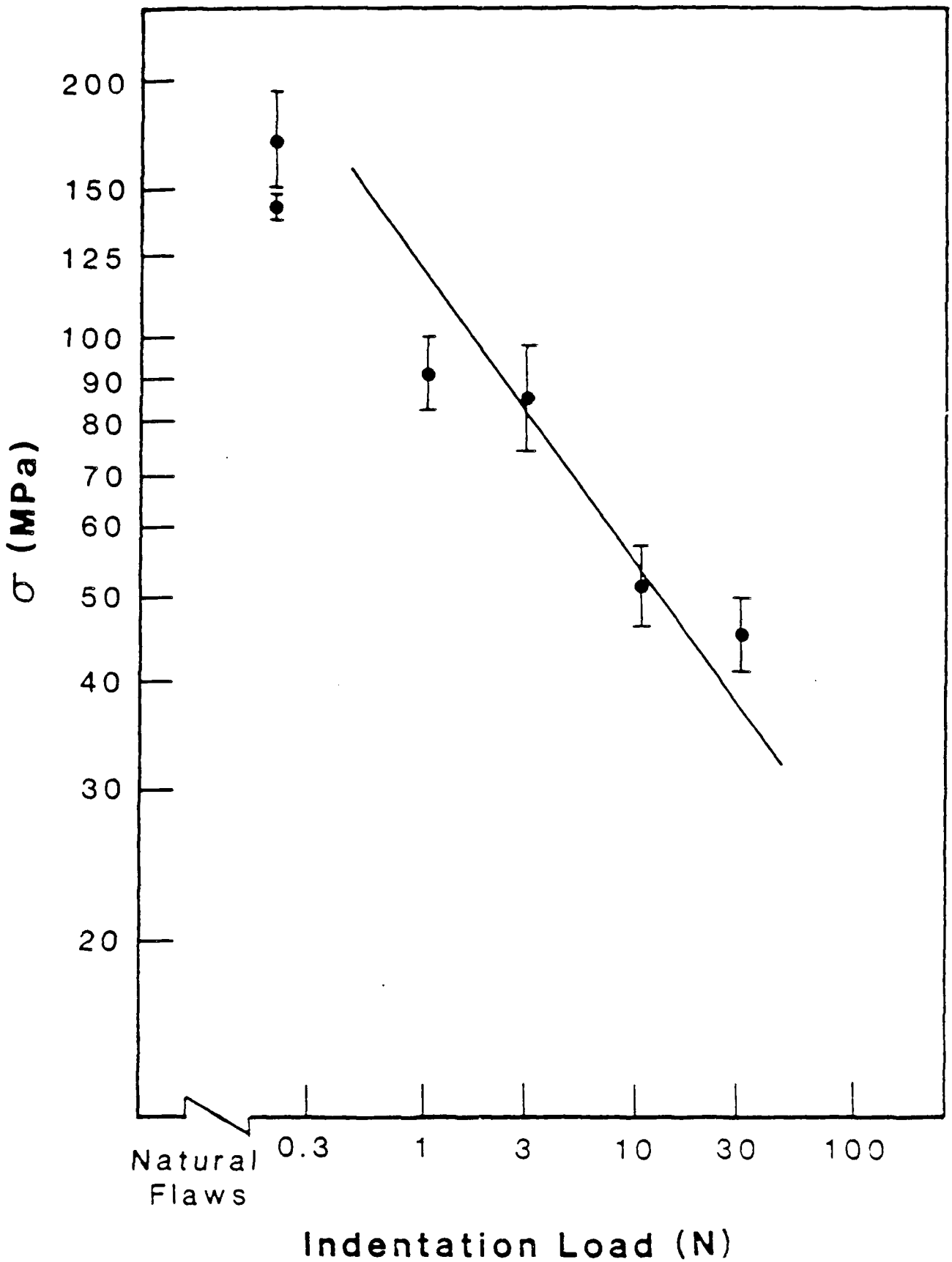

Figure 4 Fracture stress-indentation load plot for T3000 (Dupont) ceramic.

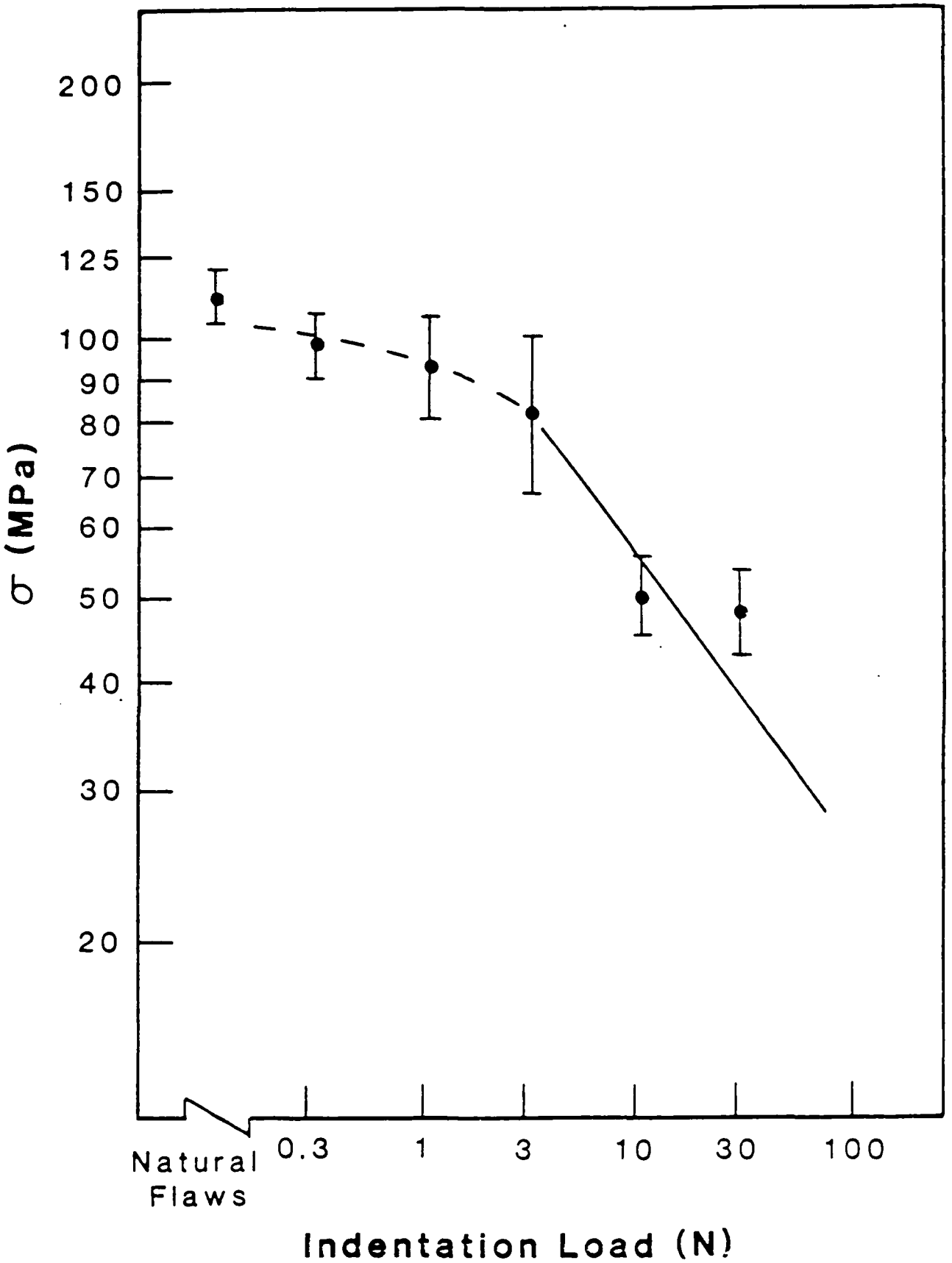

Figure 5 Fracture stress-indentation load plot for XL282 (Dupont) ceramic. Note the strong effect of microstructure in this material.

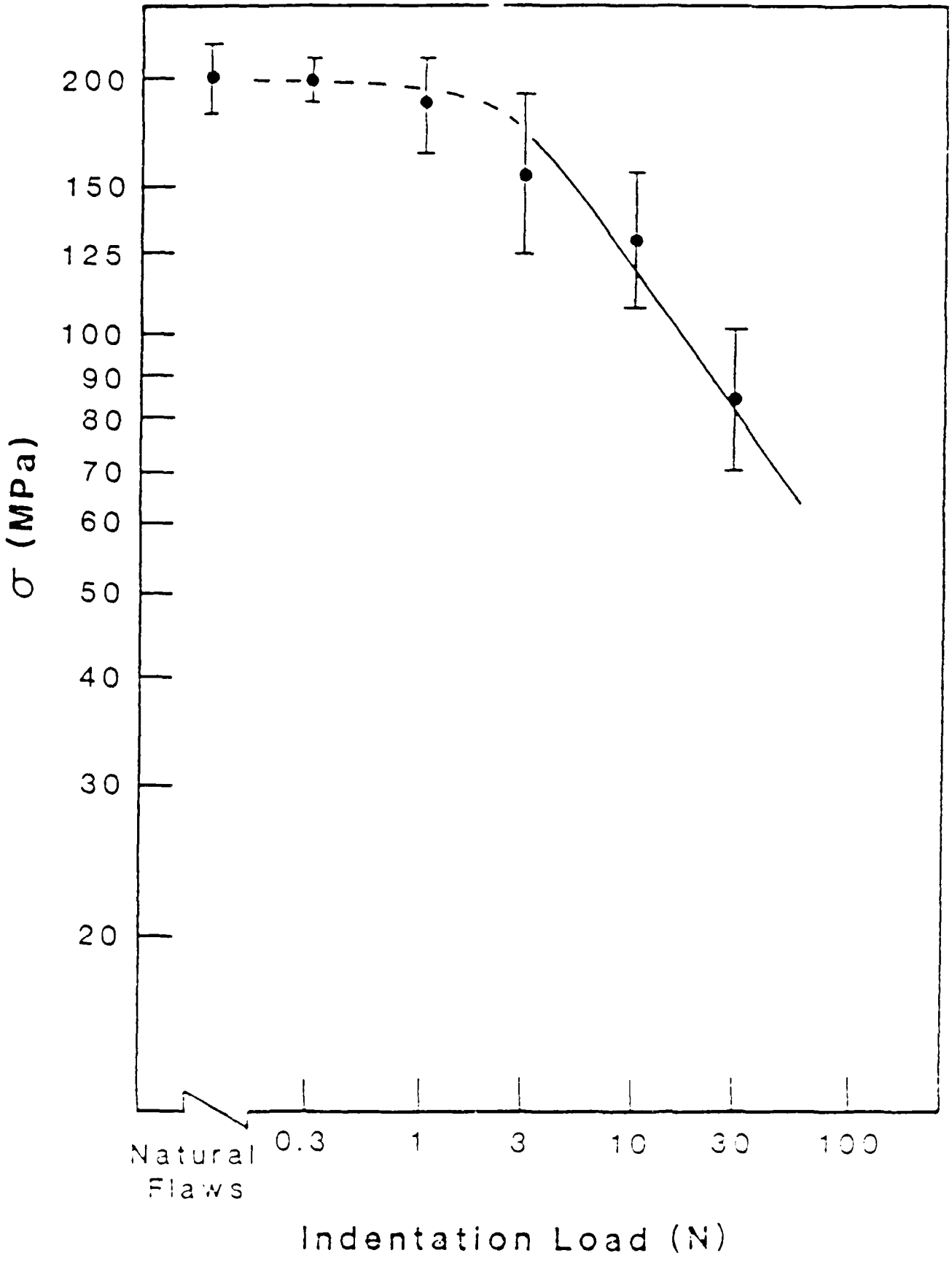

Figure 6 Fracture stress-indentation load plot for BL172HD (Dupont) ceramic. The strong effect of microstructure is hypothesized to be due to the presence of isolated large grains in the material.

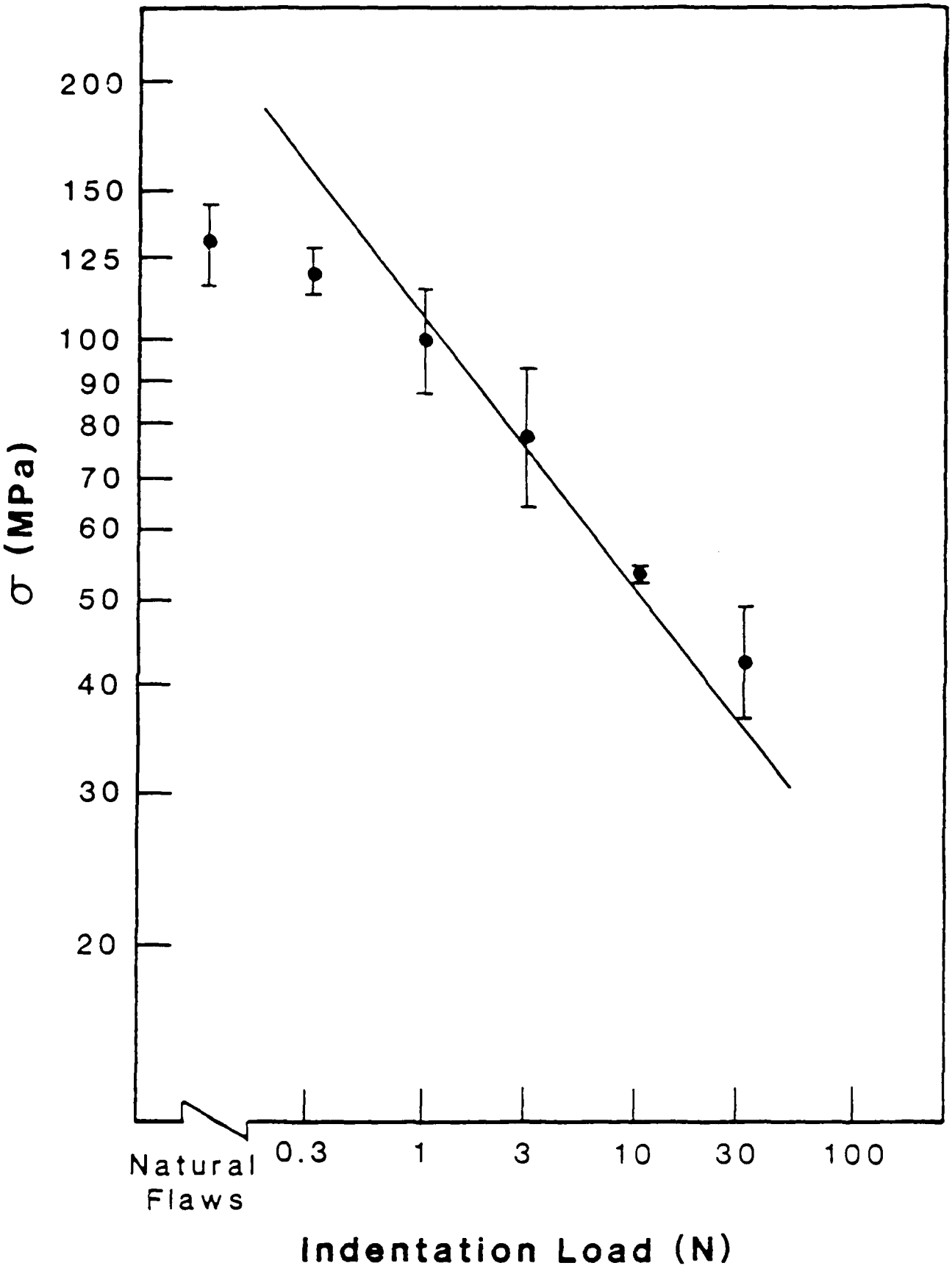

Figure 7 Fracture stress-indentation load plot for XL802 (Dupont) ceramic.

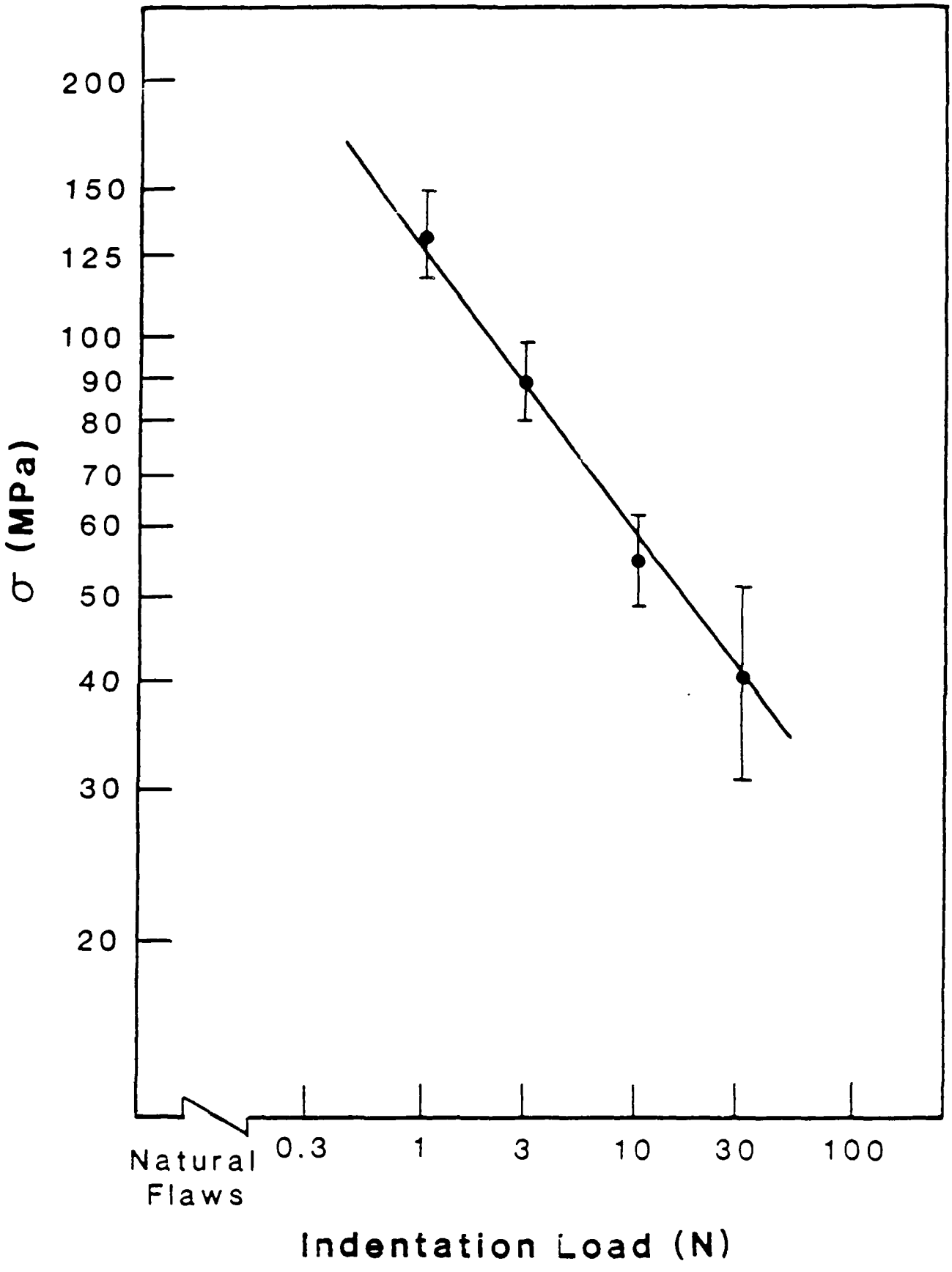

Figure 8 Fracture stress-indentation load plot for PL802 (Dupont) ceramic.

Proceedings of the TMS-AIME

Fall Meeting, Toronto, Canada

1986

ENVIRONMENTALLY ENHANCED CRACK GROWTH IN GLASS MODELED BY LATTICE GREENS FUNCTIONS

G. S White, E. R. Fuller, and R. M. Thomson

Center for Materials Science

National Bureau of Standards

Gaithersburg, MD

20899

SUMMARY

Lattice Greens functions are used to develop a very physical picture of environmental effects associated with fracture in glass. The development is proposed to be applicable in all cases where the chemical activity takes place locally at the crack tip, and where dislocation processes do not participate. In the particular case studied, the chemical reaction lowers the surface energy substantially, and gives rise to an extended region of thermally activated crack growth. Experimental results provided in the paper are interpreted in terms of the model.

KEY WORDS

Environmental fracture, Lattice Greens functions, Slow crack growth, Glass, Crack tip chemistry.

I INTRODUCTION

Brittle materials provide a good model for the study of the effect of external environments on the bond breaking process at the crack tip, because in these materials all complicating effects due to dislocations are absent. Within this class of brittle materials, the silicate glasses have been the most studied, and some of the details of the chemistry at the crack tip have been clarified.

In the glasses, the effect of water is to lower the Griffith surface energy, , substantially, because the dangling bonds created by the cleavage are saturated by the external chemical species through the formation of siloxane and similar groups on the surface[1]. Intimately associated with the change in , the interaction of water and other molecular species with the crack tip bonds of the glass induces a characteristic "slow" crack growth over a substantial range of applied stress intensity factor corresponding to many orders of magnitude in velocity[2,3]. In inert environments, there is, at best, only a limited slow crack growth region for cracks in any of the glasses. When observable at all, the slope of the v(k) curve in this intrinsic region is relatively steep.

In this paper, we will address the glass problem in some detail using atomistic theories developed earlier, with the hope that the insights to be gained will not only be of use in understanding the problem of chemically enhanced fracture in brittle materials but that the general results may also be of interest for metals, when the chemical effects in metals can be

localized to the crack tip. We will attempt to model these phenomena in terms of the lattice Greens functions for a crack[4].

II LATTICE GREENS FUNCTIONS.

The Greens function for a lattice with a crack in it allows us to write the displacement, u_0, of the atom at the center of a crack as shown in Fig. 1 in the form

$$u_0 = g_{00} F - 2 g_{0N} f \tag{1}$$

and the displacement, u_N, for the atom at the tip of the crack as

$$u_N = g_{N0} F - g_{NN} f - g_{N,-N} f \simeq g_{N0} F - g_{NN} f \tag{2}$$

Here g_{ij} is the Greens function matrix, and it is symmetric in i and j. F is the externally applied force on the central atom pair, and f is the force holding the atom pair together at the crack tip. These crack tip forces are in fact the nonlinear bond forces, $f(u_N)$, and they will be assumed later to be modified by the external chemical attack. The Greens function matrix is a set of constants which gives the compliance of the linear lattice system, and the method for computing these constants has been developed by Hsieh and Thomson[5]. The specific values for g_{ij} depend upon the type of crystal lattice, and vary monotonically on the inverse length of the crack, as indicated for g_{00} in Fig.

Otherwise, for us, the numerical values of these constants are not required; it suffices that they exist.

The solution of the coupled set of equations, (1) and (2), is quite simple, and can be described in conjunction with the help of the sketches in Figures 2 and 3. To begin, we assume that f=0 in (1). Then u_0 is simply a linear function of F, and solutions for different crack lengths are plotted schematically in Fig. 2. We note that the compliance of the lattice must decrease, as the crack increases in length, as shown. Consider, however, what must happen as the external force, F, is increased for a fixed crack length, N. The force on the atom bonds at the crack tip must increase, and if these bonds are considered to have finite strength, then at some value of F, they must break. The crack then jumps to the neighboring compliance line as in Fig. 3, i.e., to crack length N+1. (In all of this, we note that, by symmetry, any event occurring at one crack tip also occurs at the other.) Likewise, in Fig. 2 for a given N, if a large initial value of F is continuously decreased, a value will be found where the first broken bond at atom pair N-1 becomes reattached, so that these atoms snap together. At this point the solution jumps to the other neighboring compliance curve, i.e., that for N-1. Of course, for physically reasonable bond force laws these bond snapping events take place continuously, and in Fig. 3, we have shown a detailed sketch of the region where the crack jumps from N to N+1.

The crack growth from N to N+1 just described will generally occur by means of thermal fluctuations, and the activation energy for making such a jump at a specified value of the external force, F, is given by the expression

$$2\Delta E \int_1^2 F\, du_0 - F\, \Delta U_0 \tag{3}$$

The integration is over the nonlinear compliance curve from point 1 to point 2 in Fig. 3. The initial and final points are given by the intersection of the horizontal line with the compliance curves. (A backward fluctuation will occur for a jump from point 3 to point 2.) The second term in (3) is the change in energy of the external system which exerts the force, F. When the horizontal line at $F=F_F$ meets the maximum of the bond curve, the crack becomes unstable for forward motion without thermal fluctuations. The energy, ΔE, is given graphically by the area under the curve from 1 to 2 shown cross hatched in Fig. 3.

If f is eliminated from (1) and (2), we can write

$$du_0 = \frac{g_{0N}}{g_{NN}}\, du_N + 2\, g_{0N} \left(\frac{g_{00}}{2 g_{0N}} - \frac{g_{0N}}{g_{NN}} \right) dF \tag{4}$$

and substitution into (3) with (1) and (2) gives

$$\Delta E = \int_1^2 f(u_N)\, du_N + \frac{1}{g_{NN}} \int_1^2 u_N\, du_N - \frac{g_{0N}}{g_{NN}} F\, \Delta u_N \tag{5}$$

This equation will be fundamental for our discussion. In (4) and (5), we have assumed that the bond function force law, $f(u_N)$, is known. In deriving (5), we use the fact that any integration over dF from state 1 to state 2 is zero. In the following, we will define a force conjugate to the energy given in (3), which is simply the integrand in (3),

$$\mathcal{J} = \frac{g_{0N}}{g_{NN}} F - \frac{1}{g_{NN}} u_N - f(u_N) \tag{6}$$

From this function, $\mathcal{J}(u_N)$, it is possible to make a graphical construction which highlights the three contributions to the energy changes at the crack tip when it jumps forward and backward. This construction is shown in Fig. 4, where the bond function is drawn as a function of u_N. The energy is again given in Fig. 4 by the crosshatched area bounded by the bond function and the load line. The load line in Fig. 4 is the graph of the first and second terms in (6). Equation (6) and Fig. 4 are particularly useful in understanding crack growth, because only the third term in (6) depends on the external chemical reaction at the crack tip. The other terms relate solely to the linear (cracked) lattice. The first term is the force exerted by the external loading machine, and the second is the "force" associated with that part of the activation energy absorbed by the linear part of the lattice when the bond at the crack tip is stretched. Furthermore, the term in F is proportional to the crack extension force, K; $K \propto F/\sqrt{N}$. In the following, we shall therefore often use F and K interchangeably. The factor, $1/g_{NN}$,

depends on the lattice crystallography, but is on the order of a bond spring constant.

The function, $\mathcal{J}$, is an atomistic analogue to the continuum crack extension force. Indeed, when the average of over a complete jump of the crack from one lattice position to the next, $\langle \mathcal{J}(u_\alpha) \rangle_{jump}$, is zero, the crack length satisfies the Griffith condition. Also, the value of $\langle \mathcal{J} \rangle_{jump}$ is the mechanical part of the driving force on the crack to move it over the barriers. Of course, in order to obtain the complete thermodynamic driving force on the crack, entropy terms must be added to $\mathcal{J}$, but these terms will not be discussed here.

III CHEMICALLY ENHANCED FRACTURE

For the fracture problem, we now assert that the velocity, v, of the crack is given by the rate of traversal of the energy barriers, and write

$$v = v_0 \exp\{-\Delta E / kT\} \tag{7}$$

We wish to compare the situation for intrinsic fracture, shown schematically by the dashed curves in Fig. 5, with that for chemically enhanced fracture, corresponding to the full curve. Experimentally, there is only a narrow range of F (or K), at best, of activated fracture in the intrinsic case. This narrow region in the intrinsic case is due to the fact that backward fluctuations intervene when the driving force, F, is lowered only a little. The velocity also has a very steep force dependence because of the relatively broad character of the f(u) curve.

That is, small changes in F create large changes in the enclosed area.

When water or water-like molecules are introduced, the chemical reaction of the water with the Si-O bond is thought to be a concerted reaction in which lone pair electrons on the one hand and proton donor capabilities on the other play an important role[3]. In brief, it is assumed that the Si-O bond is little affected by the water until the Si-O bond achieves a critical stretch below the maximum in the intrinsic Si-O bond function. At this point, the bond breaks suddenly with formation of the Si-OH. As the Si-OH is formed, the OH groups on the two incipient surfaces repel each other, so the final stage of bond breaking is thought to be very steep with a negative region as shown in the sketch in Fig. 5. Of equal importance to the change in shape in the bond function near its maximum is the fact that the reversefluctuations, in which a water molecule is desorbed and the Si-O bond reattached, occur only with high energy, so the reverse reaction occurs sensibly only for very low values of F.

It is clear from the diagrams in Fig. 5 that quantitative results for the velocity law depend on the details of the particular force law at the tip and its modification by the chemical reaction. However, suppose we are in a region of the bond stretch not too close to $F=F_F$, and the force function is relatively linear. Then from the geometry sketched for the bond function in Fig. 5, the activation energy is approximately quadratic in the difference, (F_F-F), and since K and F are proportional,

8

$$\Delta E = A\left(K_F - K\right)^2 + \cdots \simeq A K_F^2 - 2A K_F K \tag{8}$$

K_F is the stress intensity factor corresponding to F_F. The constant A depends on the g_{ij} and the force law parameters. The linear approximation is valid when $K/K_F \ll 1$. Thus, from (7) and (8),

$$\frac{d \ln v}{dK} = \frac{2A}{kT}\left(K_F - K\right) \simeq \frac{2A}{kT} K_F \tag{9}$$

It follows from our discussion of the chemistry at the crack tip as depicted in Fig. 5 that because of the change of shape of the bond function under chemical attack, the constant, A, in (9) is lower for chemically enhanced fracture than for intrinsic fracture. Thus, for chemically enhanced fracture, (9) and the sharply lowered rate of backward reactions predict a broad regime of slow crack growth, with relatively low slope.

Experiments to be described more fully in the next section have explored a variety of molecular species similar in their chemical behavior to water. If all these molecules react with the Si-O bond in the same general linear region of the bond function, then the different cases would be as sketched in Fig. 6. That is, the shapes describing the activation energies in Fig. 6 are both similar geometric figures, described by the same material parameters. Since each molecular species will have a different reactivity with the Si-O bond, the break point of the bond will take place at a different value of F. So, for a given value of F, different velocities will be predicted by (7). However, as shown in Fig. 6, <u>for the same value of ΔE</u>, and hence

for equal velocities, the slope as given in (9) will be the same. Thus the model predicts that the curves for different molecular species will simply be shifted horizontally on a plot of lnv versus K.

There are various ways in which the simple considerations given above might be extended. For example, within the limits of the model, if the reacting molecular species break the Si-O bond in the upper nonlinear portion of the bond function, f(u), then the slopes of the lnv versus K would be expected to be higher than for those breaking the bond in the linear region.[4] See Fig. 5 for comparison.

IV COMPARISONS WITH EXPERIMENTAL DATA

The model outlined will now be compared with a number of experimental results. The most basic of these is the change in slope observed in crack growth data between curves obtained in an inert environment as opposed to those obtained in an active environment, coupled with the fact that in an active environment, crack growth occurs for much lower relative K values. Fig. 7 shows these results for fused silica. In the figure, crack growth in dry nitrogen occurs at higher K values and the slope of the curve is steeper than in active environments

such as distilled water.[2,3] These results provide the central justification for the theory we have developed.

An inspection of the environmentally enhanced region suggests that a linear lnv versus K relationship (see Eqn. (9)) is approximately valid over most of the range observable. Attempts have been made to fit this region to various functional forms to infer the actual shape of the f(u) curve. However, because of the lack of sufficient precision in the data, no predictions have been possible. Thus, the linear approximation in (8) and (9) are consistent with the data.

More interesting is the behavior of vitreous silica in environments of varying reactivity. (Relative reactivity is inferred from the relative positions of the crack growth curves along the K-axis.) Crack growth data have been obtained in water, ammonia gas, hydrazine, and formamide[3], listed in decreasing order of reactivity (see Fig. 7). The data for water and ammonia gas are colinear. Although the curves generally are displaced along the K-axis, their slopes are all equal. This suggests that the concerted reactions at the crack tip for the various environments all occur in the linear region of the f(u) function, as discussed in connection with Fig. 6 in the previous section. Therefore, the model described above is consistent with the observed crack growth data in vitreous silica for all the listed environments.

In addition to vitreous silica, crack growth data have been obtained in silicate glasses in which the Si-O bonds have been modified by the addition of alkali ions.[6] The resulting crack

growth curves are much more complicated than those in vitreous silica, but their slopes from environment to environment tend to change in a manner consistent with reactions in the nonlinear region of the f(u) curve, as discussed in the previous section. Further work to evaluate these changes is currently under way.

V CONCLUSIONS

We have indicated how the effects of environmentally enhanced fracture can be modeled in terms of lattice Greens functions. Essentially, the key to the simplicity of the method lies in the way the intrinsic bond force function, f(u), may be decoupled from the mechanical force terms describing the response of the rest of the system. This allows us to incorporate the influence of chemical interactions via a modification of the bond function at the crack tip. The effects of different environmental molecular species on the crack velocity characteristics can then be accounted for by means of a very simple construction--Fig. 5.

In the experimental results considered in Sect. IV, we confined our attention to the simplest possible cases. In these cases, the influence of the chemistry gives rise to predicted changes in the v(K) plot.

In spite of the simple physical picture presented here, however, the chemistry of cracks in glass is not an elementary science, and other observations suggest more complex behavior. Also, other interpretations than given here are being pursued.[7] Thus, the comparative study of different molecular species

interacting with cracks in various glasses is still a very active field.

A subject not discussed in this paper is the behavior of glass in the lower threshold region. On the basis of our model, adsorption/desorption reactions in equilibrium are, in principle, possible there. However, a more complex picture seems to be developing associated with healing of the crack over the chemically adsorbed molecules. Working out the physics and chemistry of these threshold phenomena is thus likely to bring in a whole set of different insights into chemically enhanced fracture.

VI ACKNOWLEDGEMENTS

It is a pleasure to acknowledge the ideas that our colleague, B. R. Lawn, has brought to this subject, and for his discussions of this paper.

FIGURE CAPTIONS

Fig. 1 Lattice containing a crack. The external force, F, is exerted at the center bond pair, and the crack tips have cohesive forces, f, holding the bonds together at the tip.

Fig. 2 Crack compliance curves. The displacement of the central atom as a function of the applied force is plotted. The displacement is linear in the force, F, and different lines are drawn for different crack lengths. The slope of a given line is $1/g_{00}$, so g_{00} is a function of crack length as shown.

Fig. 3 Compliance curve detail. At a critical bond stretch on crack length, N, (near label 1), the bond at the crack tip breaks, and the crack jumps to the curve corresponding to a crack of length N+1. The cross hatched regions correspond to activation energies of forward and backward motion, according to equation (3). That is, the area from 1 to 2 is a forward activation energy, and that from 3 to 2 is a reverse activation energy.

Fig. 4 Crack activation energy according to Eqn. (6). The energy to jump from one lattice site to the next is again given by one of the cross hatched portions. The bond function is given by the curved line, and the first two terms in (6) are represented by the straight line. This line will be called the load line. The intercepts shown define F_F and F, and the quantities Δu_N are important in determining the stress dependence of the crack growth law.

Fig. 5 Comparison of intrinsic and chemically assisted fracture. The intrinsic curve is shown dashed while the chemically assisted curve is shown full. Singly hatched regions represent activation energies for forward (bond breaking) fluctuations while doubly hatched regions represent activation energies for reverse (bond healing) fluctuations. The figure shows schematically how the force (F) corresponding to a specific forward activiation energy decreases in the chemically assisted case (F_E).

Fig. 6 Comparison of two similar molecular reactions at the tip, showing equal stress dependence. The hashed areas shown are equal. Therefore the forces F_a and F_b correspond to the same velocities in the environments a and b. The separations Δu_a and Δu_b are also equal, due to the linear nature of f(u) where the reaction takes place. Therefore, the corresponding lnv vs K curves should have equal slope, but environment b should be displaced to higher K from environment a.

Fig. 7 Experimental crack growth data of vitreous silica in different environments: water (Δ), ammonia gas (o), hydrazene (——), formamide (·····), and N_2 gas (— · —). After Michalske and Freiman. [3]

REFERENCES

1. R. K. Iler, The Colloid Chemistry of Silica and Silicates, p. 234, Cornell Univ. Press, Ithaca, NY, 1955.

2. S. M. Wiederhorn, E. R. Fuller and R. M. Thomson, Metal Science, 14, 450, (1980).

3. T. A. Michalske and S. W. Frieman, J. Am. Ceram. Soc., 66, 284, (1983).

4. R. M. Thomson and E. R. Fuller, Fract. Mech. of Ceramics, 5, 253, ed. R. C. Bradt, et al, Plenum, New York, 1983

5. C. Hsieh and R. M. Thomson, J. Appl. Phys., 44, 2051 (1973)

6. G. S. White, D. C. Greenspan and S. W. Freiman, submitted to J. Am. Ceram. Soc.

7. T. A. Michalske and B. C. Bunker, J. Appl. Phys. 56, 2686 (1984).

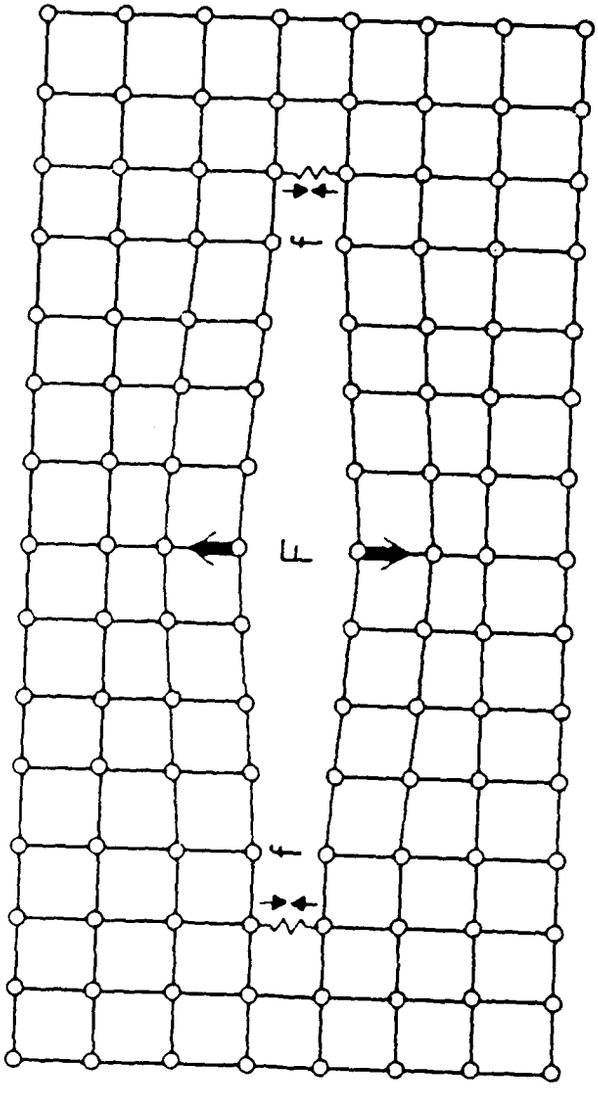
F

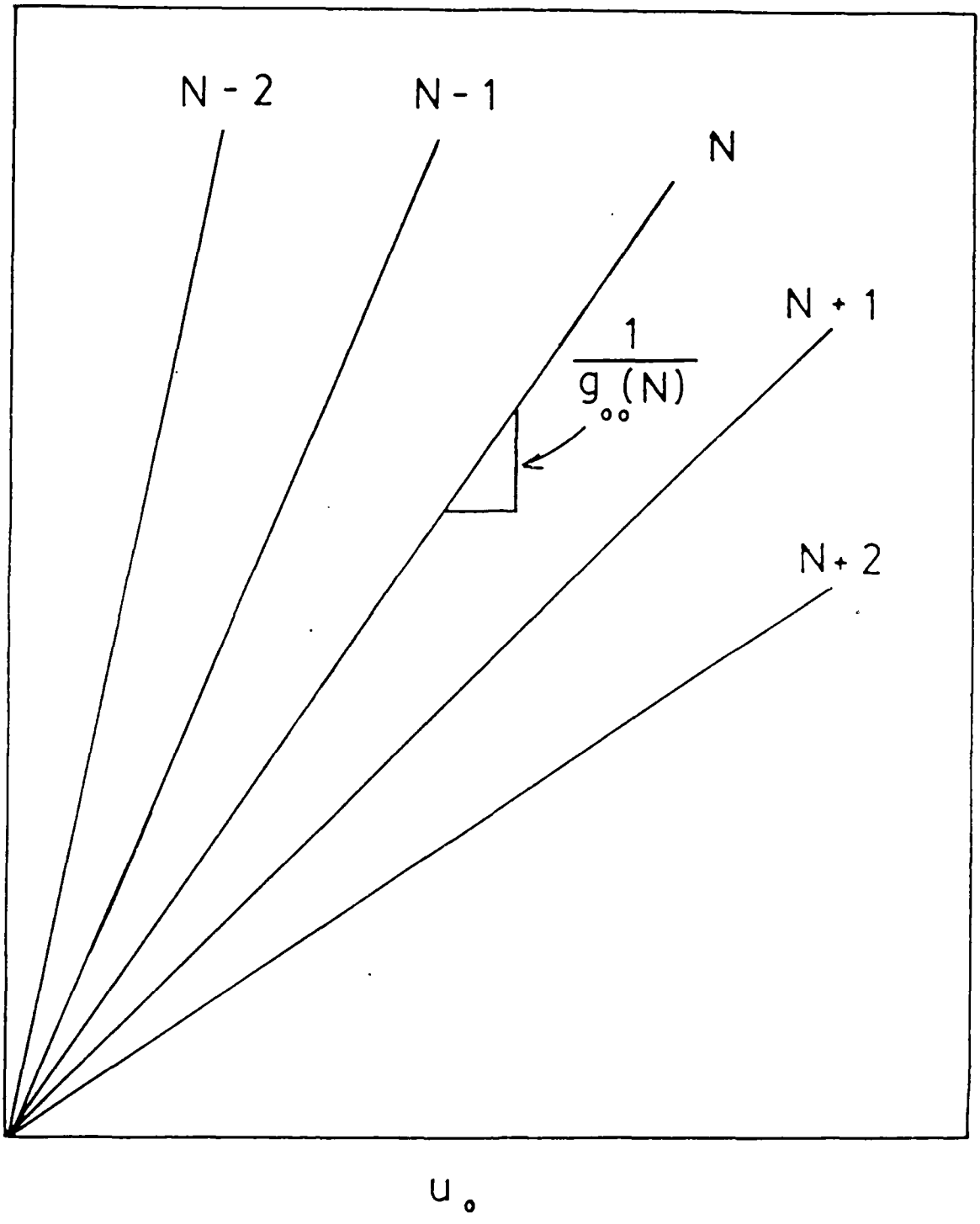
N - 2
N - 1
N
N + 1
N + 2
$\frac{1}{g_{oo}(N)}$
Force
u_o

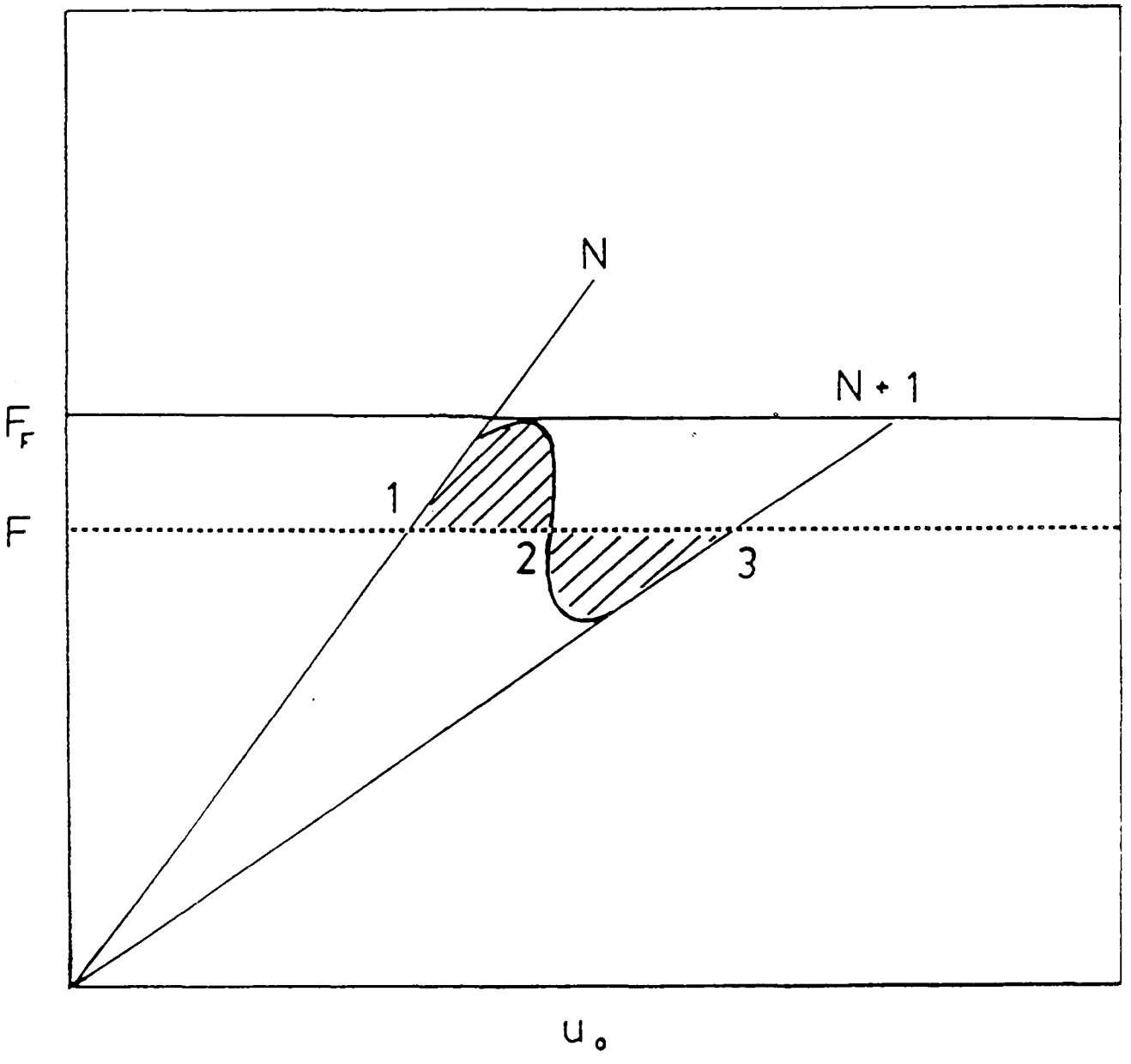
N
N + 1
F_F
F
1
2
3
u_o

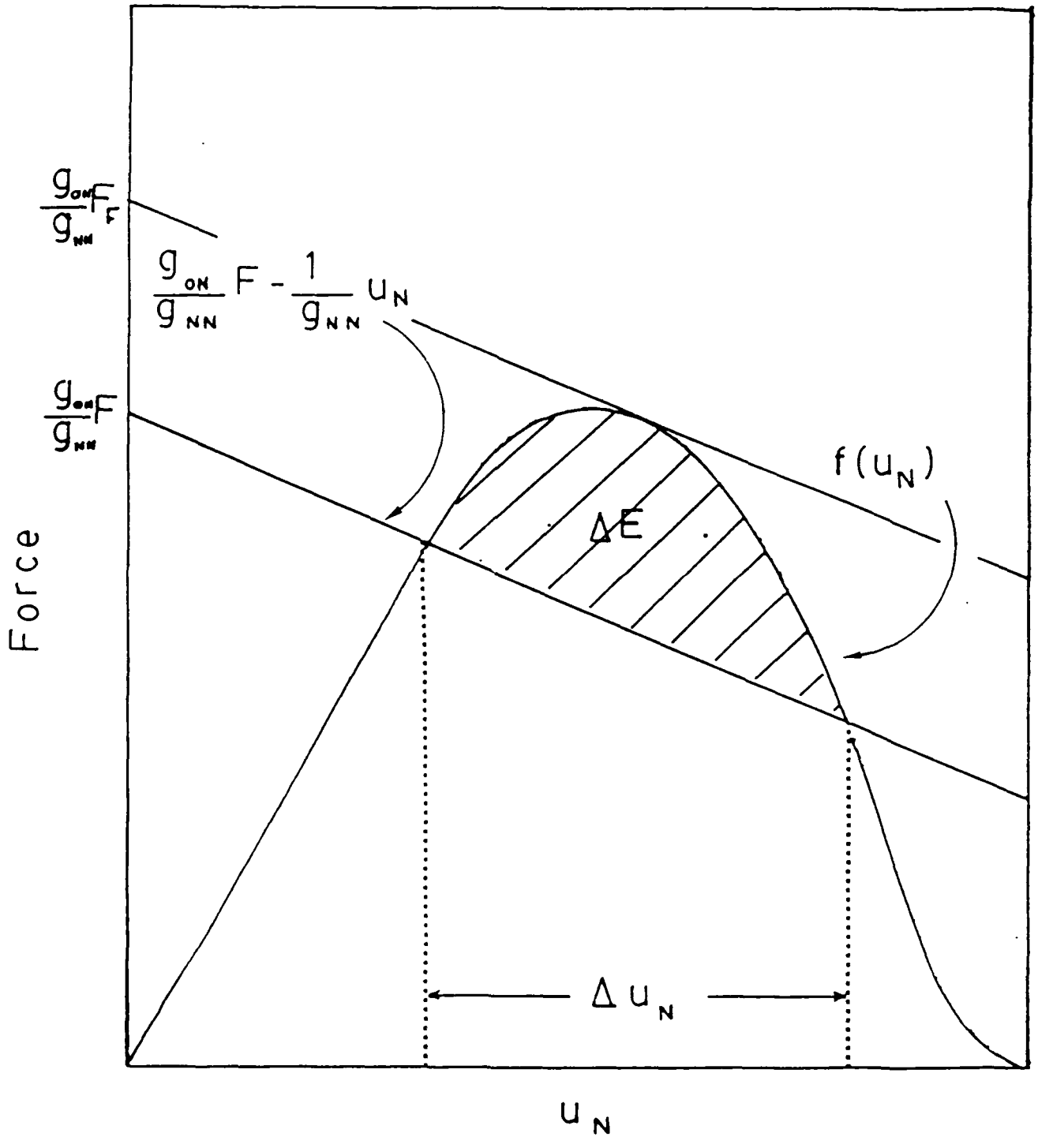
$\frac{g_{ON}}{g_{NN}} F$
$\frac{g_{ON}}{g_{NN}} F - \frac{1}{g_{NN}} u_N$
$\frac{g_{ON}}{g_{NN}} F$
$f(u_N)$
ΔE
Force
Δu_N
u_N

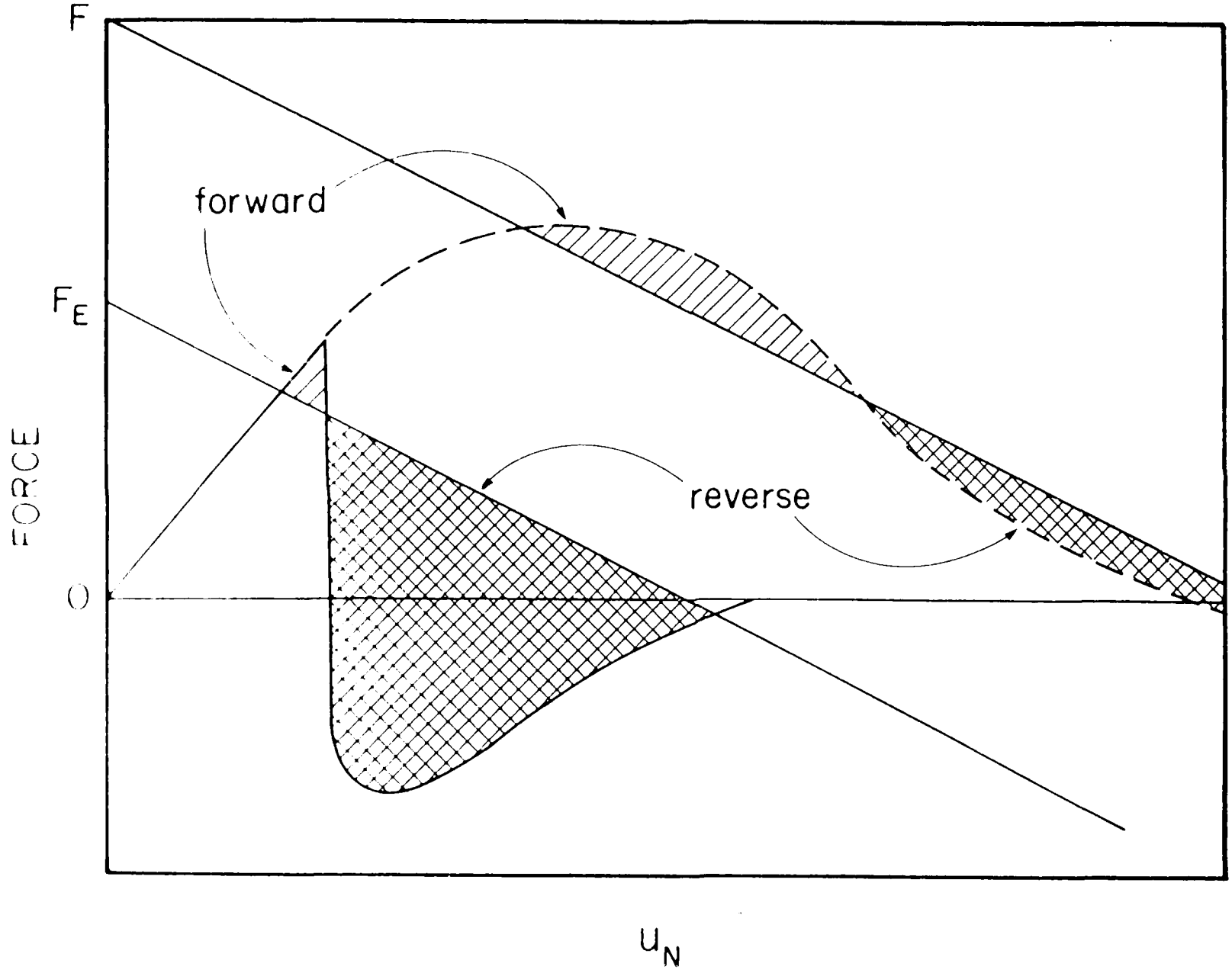
F
forward
F_E
FORCE
reverse
0
u_N

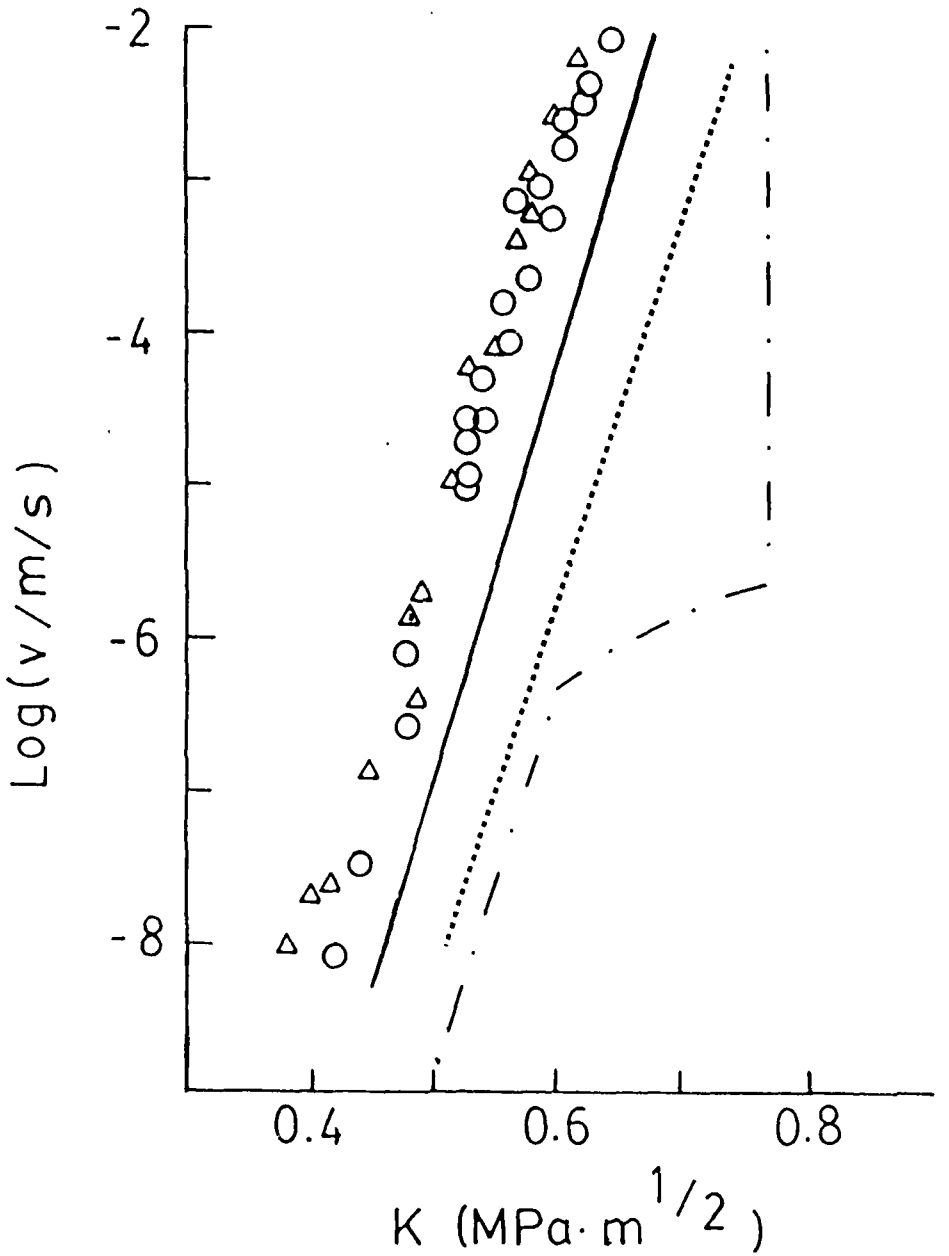
-2
-4
-6
-8
Log(v/m/s)
0.4
0.6
0.8
K (MPa·m^1/2)

Proceedings of Drip II: International

Symposium on Defect Recognition

and Image Processing in III-V Compounds

Monterey, CA

April 1987

STRAIN PATTERNS IN GALLIUM ARSENIDE WAFERS: ORIGINS AND EFFECTS

Richard A. FORMAN[1], James R. HILL[1], Michael I. BELL,[1] Grady S. WHITE[1],
Stephen W. FREIMAN[1], and William FORD[2]
[1]National Bureau of Standards, Gaithersburg, MD 20899
[2]Harris Microwave Corp., Milpitas, CA 95035

ABSTRACT

Using the rapid x-ray topographic system described earlier (in DRIP I), we have examined a large number of LEC GaAs wafers, both commercial and research, and have been able to identify the sources of some of the observed patterns. We have also studied the effects of the inhomogeneous strain on the fracture properties of the wafers. The high gradients of strain cause deviations from expected crack growth behavior in fracture tests. These deviations include crack velocity variations, and crack tip deflections. The grown in defects cause point-to-point irreproducibility in hardness and toughness values for this material. Sequential wafers exhibit closely related topographs and similar fracture properties. Inclusions have been identified in indium-doped wafers and produce a characteristic topographic pattern when the inclusion lies in the wafer under study. A characteristic strain pattern propagates away from the inclusion and produces annular rings in later wafers. The relaxation of the bow-tie strain pattern surrounding the inclusion to the annular ring pattern is likely related to the thermoelastic stress patterns described by Jordan et al.

INTRODUCTION

We have previously described a sample laboratory system for routine x-ray topographic inspection of semiconductor wafers.[1] We have since continued exploratory studies to examine the generic defect structures observed in gallium arsenide (GaAs) wafers, and to correlate these topographic results with other data.

Samples representative of current GaAs production have been obtained from a number of sources, both commercial vendors and research laboratories. In several cases, samples from different regions of the same boule were studied and used to examine defect propagation. The wafer thicknesses were nominally 500 μm. All topographs were taken with CuK_α radiation.

Crack propagation studies were also performed on samples taken from a sequential set of liquid-encapsulated Czochralski (LEC) GaAs wafers. Breakage remains a significant factor for GaAs device fabrication, and our studies were intended to address the materials and defect aspects of crack propagation. Hardness measurements were also made. In the absence of strain or other defects, hardness would be uniform over the wafer surface.[2] Cracks would also be expected to grow smoothly along the known [110] cleavage planes.

Currently available LEC GaAs wafers do not behave in this way; the nonuniform crack behavior correlates well with the inhomogeneities observed in the x-ray topographs.

Inclusions are also an occasional problem in GaAs boules, and are generally regarded as being produced occasionally by an unexpectedly large growth rate fluctuation. We have been able to examine, in successive wafers from the same boule, the topographic patterns associated with the presence of an inclusion, and the subsequent strain pattern which propagates along the boule. While the inclusions studied here were found in indium-doped materials, we have observed similar x-ray topographic patterns in undoped and chromium-doped GaAs wafers, suggesting the same underlying cause.

Many of the LEC GaAs wafers we have examined display subgrains. Examination of a set of ten wafers from near the end of one boule has allowed us to measure the effects of competing grain growth and the development of significant sharp localized strain patterns at the intersections of the subgrains. These results suggest that whole boule annealing to relieve strains may have a fundamental limitation when subgrain structure is important.

EXPERIMENTAL

All of the x-ray topography was performed with the double-crystal system described earlier.[1] All measurements were made using a Si (100) wafer monochromator crystal on the (224) plane with CuK_α radiation. A lead aperture mask was used to isolate the $CuK_{\alpha 1}$ line; all the topographs were taken in the reflection mode and various different resolution emulsions were used with or without x-ray intensifying screens. All topographs shown here are positive images. The wafers were as supplied by the manufacturer without any etching to remove possible damage. For most of the work, the (422) Bragg reflections were used in the parallel (+ -) geometry; this reflection samples a depth of 5.5 μm for GaAs single crystal samples.[3] In some cases the (440) reflections were also studied to give further information about the inhomogeneous strain distributions. Because of the divergence properties of the monochromatic x-ray beam in this apparatus, the use of Bragg reflections at 45° to each other about the surface normal is sometimes useful to more completely quantify the strain patterns.

Two types of mechanical property tests were made: indentation tests using a Vicker's diamond in a standard hardness testing machine and macroscopic crack growth measurements using a double cantilever beam (DCB) apparatus. For the first type of test, indentations were made with the diamond indenter oriented to produce cracks running along the cleavage planes. Indentations were made in air and lengths were measured of cracks

emanating from the corners and the sides of the indentation impression. Hardness values were obtained from measurements of the diagonal length of the indentation impression.[2,4] The values of the measured crack lengths reflect the sum of the residual stress associated with the indentation and the remanent local stresses produced during growth, slicing, and polishing of the wafer.

For the DCB tests, specimens 12.5×50 mm were cleaved from the wafers. A crack was initiated at one end of the specimen by applying a 1.75 Newton load to the specimen with a Knoop diamond indenter mounted in a universal testing machine. Next, the specimen was glued to two aluminum arms and mounted in an environmental chamber using an apparatus described elsewhere.[5] Loads were then applied to the aluminum arms to cause the crack to propagate. The advantage of the DCB geometry is that the driving force is independent of crack length. Therefore, for a given applied load, the crack will run at a constant velocity, unless there are residual stresses within the specimen. Crack velocities were determined by measuring the distance traveled over a given time using a traveling microscope and a stopwatch. Velocities between 10^{-10} and 10^{-2} m/s can be measured in this way.

RESULTS AND DISCUSSION

The wafers selected for the crack growth experiments are representative of current production undoped LEC material intended for device fabrication. The particular set of ten examined were from the tail section of a boule but were device quality wafers. The x-ray topographic patterns observed in these wafers are qualitatively the same as those we have observed in wafers from other manufacturers independent of position in the boule.

Fig. 1 shows reflection topographs of two of these wafers. Allowing for kerf losses, we estimate that these wafers were separated by approximately 5 mm along the boule axis. The topographs were taken at the position of the rocking curve where the average intensity from the central 15 mm of the crystal was a maximum. Because the subgrain structure of the two wafers is so similar, the bright areas of the two topographs display many of the same features. The mottled nature of the topograph is produced by the dislocation networks which are well-known in LEC GaAs and whose spatial structure is more commonly examined in transmission topography.[1,6] Subgrains are also prominent in the topographs and the relative rates of grain boundary motions during growth for the various grains can be observed by comparison of the topographs.

A crack propagation study sample was taken from the wafer shown in Fig. 1a; Fig. 1c

projects the geometry of the DCB specimen onto the topographic features of that specimen wafer. We had believed that the higher crystalline uniformity of this region of the wafer might allow reliable crack propagation studies to be made.

The crack in the DCB test specimen was propagated toward the center of the wafer. When the crack reached the region marked (j), it was deflected at a right angle and ran off the side of the specimen. As the figure shows, the site of the crack deflection coincides with indications of residual strain determined by the x-ray topography. Cracks propagated in DCB specimens cleaved from 3 of the 10 consecutive LEC wafers all exhibited fluctuations in crack velocity and direction. In all cases, these fluctuations led to failure of the specimens part-way through the crack study.

Indentation crack lengths were also correlated with the topographs. Fig. 2 is a plot of the tip-to-tip crack lengths as a function of position for a row of indentations which crosses a sharp residual strain line in the wafer. The vertical dashed line in the figure corresponds to the position of the strain line of the x-ray topograph. The cracks run approximately perpendicular to the strain line. Uncertainty in the crack lengths is about 1μm. The crack length at the strain line is much larger than the background crack length values. As the figure shows, there is another position in the row of indentations at which the crack length deviates from the background value. There is no corresponding topographic data available for this second case. However, parallel rows of indentations provide similar results.

The correlations between the observed crack growth behavior and the residual strain lines indicated in the x-ray topographs suggests that the strain sites are also locations of residual stresses in the wafers. As Fig. 2 shows, the crack length changes from the background value to a higher value at the strained site, corresponding to a tensile residual stress. At other positions near the strained site, there exist compressive residual stresses, required to maintain a net zero stress state. Fig. 2 shows both a tensile and a compressive region away from the strained site detected by the topograph. Unfortunately, these stresses were located in a region which did not meet the Bragg reflection criteria at any of the tested angles, so no topographic information was available.

The average hardness of the specimen was determined to be 3.6$\pm$0.3 GPa. Although variations in the hardness were observed, they fell within the uncertainty of the measurement technique. Therefore, no correlation of the hardness values with the observed residual strain line was possible.

The inevitable grain growth which occurs as the boule grows can be seen to be a source

of significant high strain areas. At the bottom of both topographs in Fig. 1a and 1b we observe two large subgrains with the region nearest 6 o'clock as an intermediate. As growth proceeds, the intermediate region decreases in size. The gradients of strain between the intermediate region and the neighboring subgrains become much larger. This high strain is related to the exact misorientation between the subgrains. Based upon our experience with a number of other wafers, such high strain gradients are often precursors of cracks, or at least of a high tendency toward cracking. The alignment of the boundaries of the highly strained area with the easy cleavage directions certainly favors cracks. We do not know whether this alignment, which we have seen in numerous wafers, is merely fortuitous or has an underlying crystallographic cause. Further study of subgrain growth is in progress and will be reported later.

Fig. 3 displays x-ray topographs of two lightly indium-doped LEC GaAs wafers taken from an early growth run of a series of indium-doping experiments. These wafers have a much lower indium content than is now typically used to harden LEC GaAs wafers. Striations, usually seen in GaAs:In[6,8] are absent, but a diamond-shaped texture is easily observed in Fig. 3a. This is the only sample we have ever seen with this texture in the topograph. This wafer was near the seed end of the boule, and the remaining pattern could be considered typical of current LEC GaAs except for the two major 'bow-tie' strain patterns near the wafer center.

These 'bow-tie' patterns are produced by a macroscopic inclusion inside this wafer. Examination with a polarizing infrared microscope system revealed a cubic habit, infrared opaque, dendritic precipitate. Very high birefringence is associated with this inclusion. The results of the infrared examination as well as chemical analysis studies of the inclusion will be presented elsewhere.[9] We believe that the inclusion is metallic indium and that the strain results from the differential thermal expansion between the gallium arsenide matrix and the inclusion. In the growth of LEC GaAs, it is well known that the material remains plastic while inside the molten cap. This means that a maximum strain occurs beyond which the material deforms, and produces dislocations. Ordinary thermoelastic stresses have been studied in detail by Jordan and co-workers and are known to be responsible for the cellular dislocation patterns found in all undoped LEC materials.[10] In this case the situation is somewhat different for the inclusions.

Examination of the highly defected wafer from the tail region of the same boule shows a number of small size high strain features (Fig. 3b). Superposition of the topographs shows

that two of these small annular ring patterns occur where the 'bow-tie' was seen in the wafer of Fig. 3a. A number of other annular rings and 'bow-ties' are also visible along with slip, lineage, and other crystal defects. We believe that the annular ring patterns are produced by stress relief of the 'bow-tie' strain at the time it passes through the molten cap. It is apparent that the patterns formed *for this defect* propagate parallel to the boule axis and do not behave identically to the thermoelastically produced cellular patterns.

The 'bow-tie' pattern which remains is likely produced by the further differential strains produced after cooling below the temperature at which the material is plastic. The large spatial extent of the strain pattern is in accord with this interpretation. While the annular ring patterns are visible far from an inclusion, we believe that the 'bow-tie' is a signature of the inclusion actually occurring in the wafer under study. We have observed annular ring patterns in numerous wafers of doped GaAs and believe it is reasonable to conclude that they also are the result of strain relief of an inclusion. Instability of growth is probably the underlying cause of the inclusions.

CONCLUSIONS

Correlations between property measurements and x-ray topographic examination have been made. For those measurements which could be influenced by strain, it would appear essential to examine residual strain patterns before beginning the property measurements.

Crack growth becomes unstable near high strain gradient regions, and reliable values of crack velocity as a function of stress intensity factor cannot be obtained. We have established that at least some of these high strain gradient regions are associated with regions of residual stresses which can be either compressive or tensile in nature. These stresses are sufficient to affect observed crack growth behavior. In addition, the existence of areas which are highly strained along easy cleavage paths can result in crack deflection and specimen failure.

Subgrain growth is also responsible for highly strained regions of wafers and is likely to remain a problem for crystal growers. Our results suggest that the tail regions of boules would likely produce wafers more susceptible to breakage than seed end wafers of the same boule. It is unlikely that the current practice of whole boule annealing will relieve these grown-in strains.

Patterns characteristic of inclusions in doped GaAs boules have been identified and a mechanism for the production of these patterns proposed. Further quantitative work in this area is clearly needed.

REFERENCES

1 R. A. Forman, M. I. Bell, S. Mayo, Rapid X-Ray Topographic Examination of GaAs Crystals, in: Defect Recognition and Image Processing in III-V Compounds, ed. by J. P. Fillard (Amsterdam, 1985) pp. 55-62.

2 A. Gonzalez, J. Jimenez, and J. A. deSala, Microhardness Cartography of Semi-Insulating LEC (Liquid Encapsulated Czochralski) GaAs Wafers, in: Defect Recognition and Image Processing in III-V Compounds, ed. by J. P. Fillard (Amsterdam, 1985) pp. 261-267.

3 S. O'Hara, M. A. G. Halliwell, and J. B. Childs, The Optimum Choice of Reflexion to Reveal Dislocations in Gallium Arsenide by X-Ray Reflexion Topography, J. Appl. Cryst. 5 (1972) pp. 401-407.

4 G. R. Anstis, P. Chantikul, B. R. Lawn, and D. B. Marshall, A Critical Evaluation of Indentation Techniques for Measuring Fracture Toughness: I, Direct Crack Measurements, J. Am. Cer. Soc., 64(9) (1981) pp. 533-538.

5 S. W. Freiman, D. R. Mulville, and P. W. Mast, Crack Propagation Studies in Brittle Materials, J. Mater. Sci., 8 (1973) pp. 1527-1533.

6 M. P. Scott, X-Ray Topography and Diffraction Imaging in III-V Compounds, in: Defect Recognition and Image Processing in III-V Compounds, ed. by J. P. Fillard (Amsterdam, 1985) pp. 41-54.

7 A. S. Jordan, A. R. VonNeida, and R. Caruso, The Theoretical and Experimental Fundamentals of Decreasing Dislocations in Melt Grown GaAs and InP, J. Cryst. Growth 79 (1986) pp. 243-262.

8 D. L. Barrett, S. McGuigan, H. M. Hobgood, G. W. Eldridge, and R. N. Thomas, Low Dislocation, Semi-Insulating In-Doped GaAs Crystals, J. Cryst. Growth 70 (1984) pp. 179-184.

9 R. A. Forman, T. Torsch, J. R. Hill, and M. I. Bell (in preparation).

10 A. S. Jordan and J. M. Parsey, Jr., The Role of Crystal Diameter and Impurity Hardening on the Threshold for Dislocation Formation in LEC GaAs, J. Crystal Growth, 79 (1986) pp. 280-286.

Fig. 1. (a) Reflection topograph of an undoped LEC GaAs wafer from the boule used for crack growth experiments. (b) Reflection topograph of a wafer approximately 5 mm farther down the same boule as that shown in (a). (c) Drawing of topograph shown in (b); the lines indicate the boundaries between the black-white contrast (areas of extinction contrast). The region marked (j) is where the crack deflected at a right angle and ran off to the side of the specimen. Indentation impressions were made in the region marked (k).

Fig. 2. Plot of indentation crack length versus indentation position. The dashed line marks the position of a residual strain line similar to that seen at the top of Fig. 1c. The results show that a region of tensile residual stress coincides with the residual strain line.

Fig. 3. (a) Reflection topograph of a lightly indium-doped LEC GaAs wafer, displaying 'bow-tie' stain pattern at the sites of inclusions. (b) Reflection topograph of a wafer much farther down (near tang end) the same boule as that shown in (a); showing remnants of the characteristic 'bow-tie' pattern of an inclusion in the center region of this Figure.

Fig 1 (a)

Fig 1 (b)

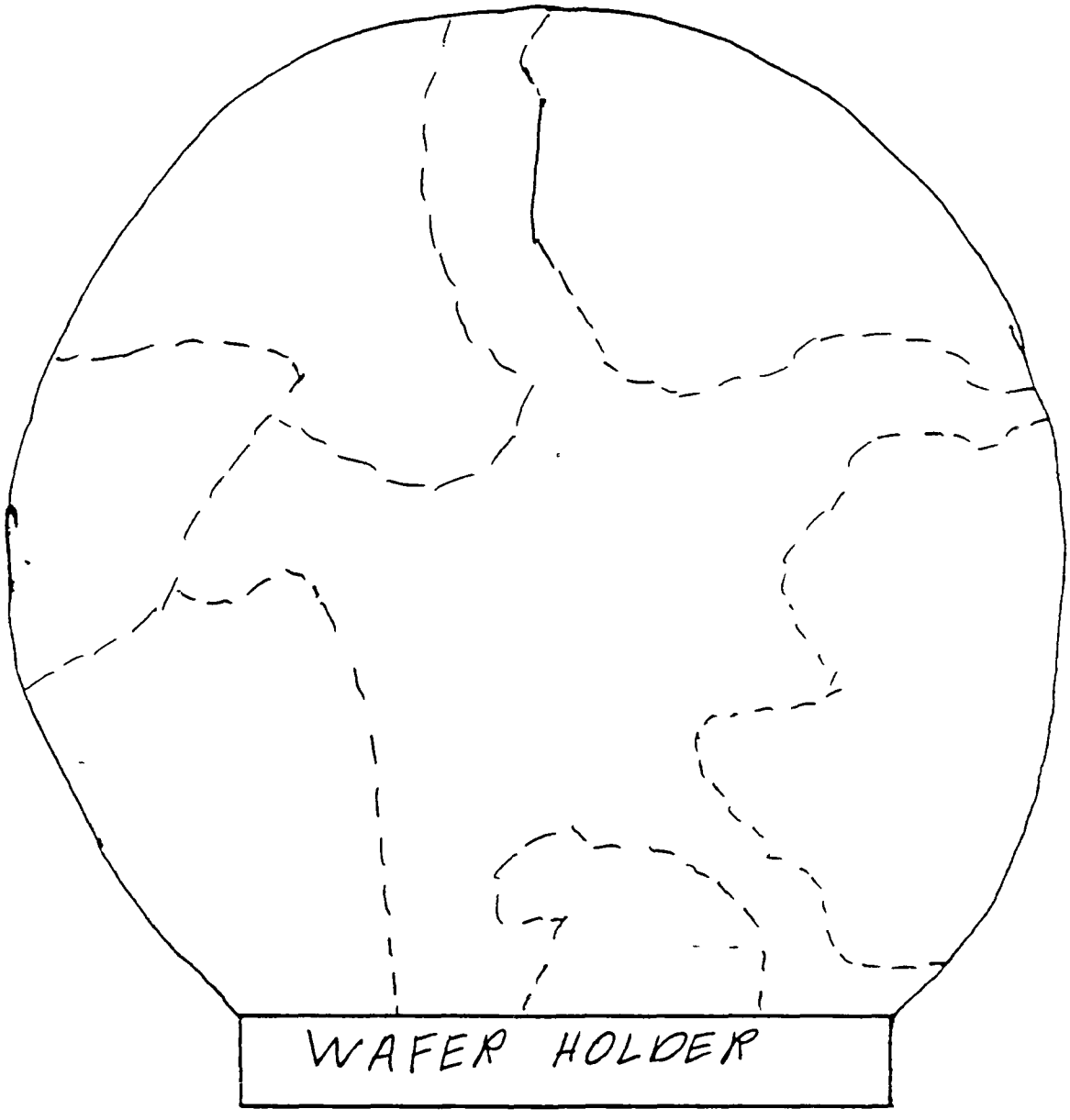

FIG. 1. (C)

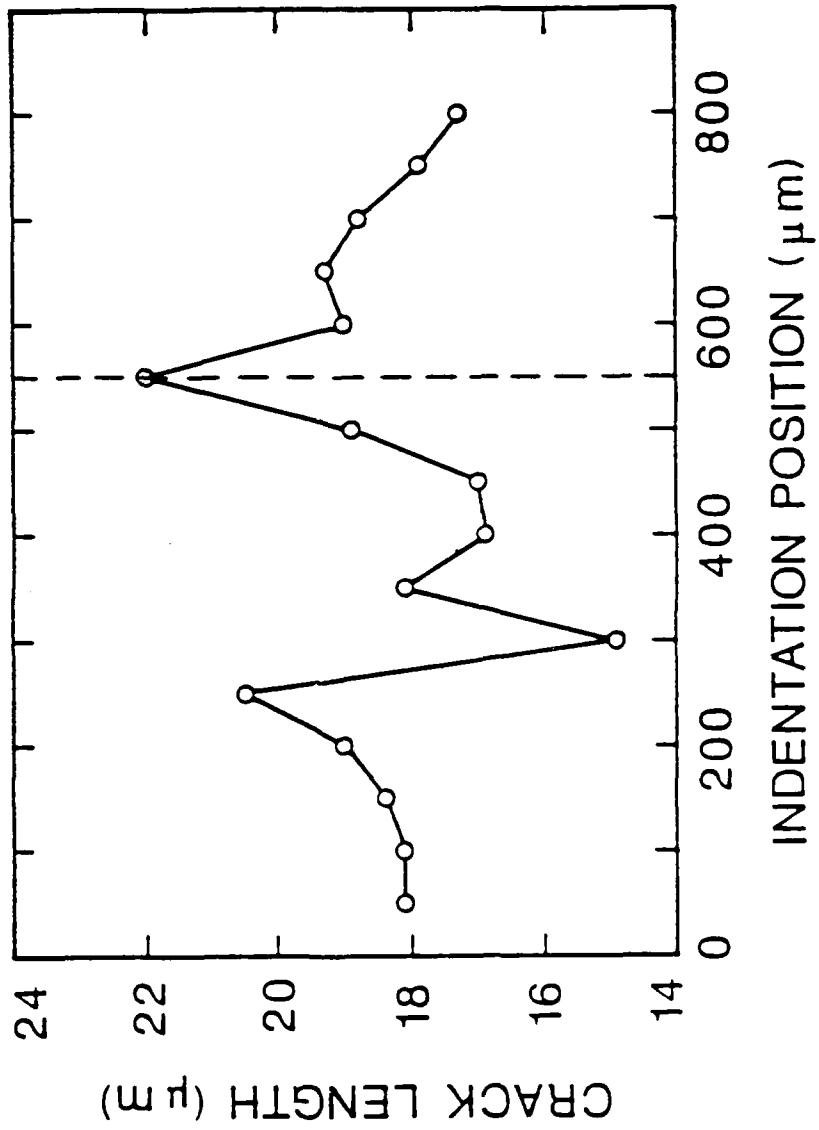
CRACK LENGTH (μm)
24
22
20
18
16
14
0
200
400
600
800
INDENTATION POSITION (μm)

Proceedings of Conference on Nondestructive

Testing of High Performance Ceramics

Boston, MA

August 1987

Proceedings of the Sixth IEEE International

Symposium on Applications of Ferroelectrics

June 1986

MECHANICAL BEHAVIOR OF FERROELECTRIC CERAMICS

Stephen W. Freiman

National Bureau of Standards
Gaithersburg, MD 20899

Abstract

This paper reviews the mechanical behavior, and in particular, the strength, fracture toughness and susceptibility to environmentally enhanced crack growth in ferroelectric materials such as barium titanate and lead zirconate titanate (PZT). Polycrystalline ferroelectric ceramics are known to exhibit a critical fracture toughness, K_{Ic}, as measured by classical fracture mechanics techniques, which depends strongly on grain size, and in the case of PZT, chemical composition and phase content. There are a number of mechanisms which can contribute to the crack growth resistance of ferroelectric ceramics. These mechanisms are discussed in terms of their dependence on variables such as grain size, composition and crystal structure. It is shown that fracture toughness models can be used to predict microstructures which should lead to an optimum in crack growth resistance for a given material.

The microstructure of a ferroelectric ceramic is shown to have a direct effect on the strength of a component as well as influence its resistance to the growth of large cracks. The paraelectric to ferroelectric phase transformation in barium titanate, PZT, and related ceramics induces internal stresses into the materials which provide an additional driving force for flaw extension. Indentation-strength procedures have been used to demonstrate the influence of these internal stresses on fracture when flaw sizes approach the grain size in the material. The magnitude of such stresses calculated from strength data is in good agreement with that predicted by dielectric measurements.

Finally, crack growth rates in ferroelectric ceramics have been shown to be accelerated by the presence of moisture in the environment. Such environmentally enhanced crack growth can have a significant effect on failures of electrical components in service, since cracks will grow with time under a static stress whose magnitude can be much less than the strength of the material. The susceptibility of each material to environmentally enhanced fracture is shown to be particularly dependent on its chemical composition.

1. Introduction

During the past few years, as new devices and applications involving ferroelectric ceramics have been developed, interest and concern over the mechanical reliability of these materials has increased. These applications can involve the dielectric as well as the piezoelectric or ferroelectric properties of the material. In this paper we will attempt to bring together a number of the concepts discussed in the literature over the past few years, and will attempt to show that the mechanical behavior of these sometimes quite different materials can be understood through the application of a few general models. The format of this paper will consist of a review of each group of materials followed by a summary which will attempt to present an overall picture of their mechanical behavior.

2. Barium Titanate

One of the most important observations regarding the fracture behavior of ferroelectric materials was made by Pohanka et al [1] in 1976. These authors found that the strength of polycrystalline barium titanate measured above its Curie temperature was approximately 50% greater than that measured at room temperature, and that this difference was essentially independent of the grain size in the material (Figure 1). Based upon this strength difference, Pohanka et al concluded that internal stresses generated during the cubic to tetragonal phase transformation added to the applied stress to lower the strength of the material at room temperature. The values of internal stress calculated from the strength difference were shown to be in good agreement with that predicted by Buessem et al [2] from permittivity measurements.

In a more recent study, Cook et al [3] followed up on this work using an indentation-fracture technique to investigate both the fracture toughness and internal stress effects in both commercial barium titanate (grain size = 7 microns) and one of the experimental materials prepared by Pohanka et al [1] (grain size = 1 micron). The advantage of the indentation-fracture procedure is that a Vickers hardness indenter can be used to create a flaw of known size and which is driven by a well characterized stress field. The results of this study are demonstrated for the commercial barium titanate in the logarithmic plot of fracture stress versus indentation load shown

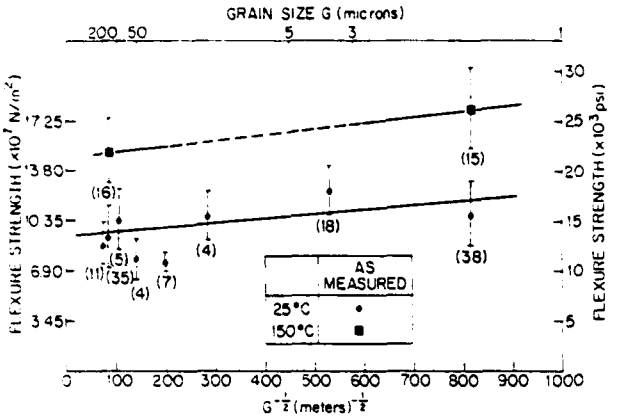

Figure 1. Flexural strength of a laboratory prepared barium titanate as a function of grain size, G. Measurements were made in silicone oil at 25° C or above the Curie temperature at 150° C. The numbers of specimens per data point are shown in parentheses (after Ponanka et al [1]).

in Figure 2. The slopes of the curves in the large indentation load regime are -1/3 as predicted from the indentation fracture model [4]. The critical fracture toughness of the material can be calculated from the position of these curves using an expression derived by Chantikul et al [4]. These calculations yield values of K_{IC} of 1.1 MPam$^{1/2}$ and 1.5 MPam$^{1/2}$ for the cubic and tetragonal material respectively. Cook et al also showed that K_{IC} decreased monotonically with temperature through the Curie point. The increased toughness of barium titanate in the tetragonal state had already been demonstrated by Ponanka et al [5], who showed that the increased K_{IC} could be ascribed to cracks interacting with 90° domains in the structure. These domains exist in tetragonal but not cubic barium titanate. A similar difference in K_{IC} above and below the Curie point was reported by de With and Parren [6] for modified barium titanate.

The deviation of the strengths at small indentation loads from the indentation model in Figure 2 for the tetragonal material is indicative of the increasing influence of the internal stresses as the flaw size decreases relative to the microstructure. The difference in strengths between the tetragonal and cubic material is approximately 56 MPa, essentially that calculated earlier by Ponanka et al [1]. Experiments performed on barium titanate made semiconducting by the additions of a small quantity of samarium indicate that the level of internal stress is not reduced by increasing the conductivity of the material [7]. This result leads one to the conclusion that the internal stresses are not due to the formation of space charges in the material.

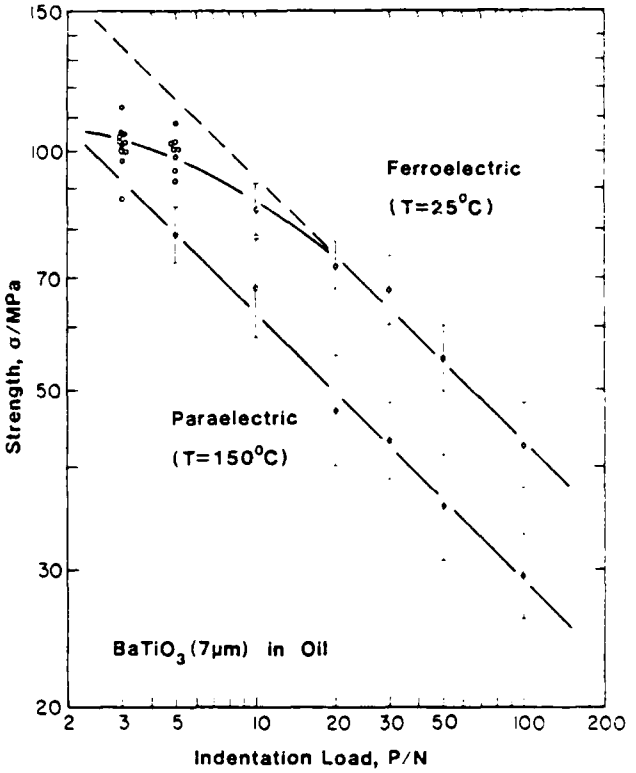

Figure 2. Flexural strength of a commercial barium titanate tested above and below the Curie temperature as a function of the indentation load used to introduce the flaw. All failures occurred from the indentation. The straight lines through the data at 25° C and 150° C represent the best fit line of slope, -1/3, following the indentation-fracture model [4]. The deviation in the 25° C data from the model is ascribed to the contribution of internal stresses (after Cook et al [3]).

It has also been shown that in the ferroelectric state, the fracture energy, γ of polycrystalline barium titanate is a function of grain size, while that for cubic material is independent of grain size (Figure 3) [8]. The grain size dependence of γ for the tetragonal material was explained in terms of a combination of 90° domain and microcracking enhanced toughening in the material. The maximum in at a grain size of 40 microns occurs due to a tradeoff between the generation of microcracks at the primary crack tip, a process which reduces the driving force on the crack, and the linking of the microcracks, which at large grain sizes produces spontaneous failure of the material. It was shown that this complex behavior could be fit to a general model for the fracture energy of non-cubic ceramics derived by Rice and Freiman [8].

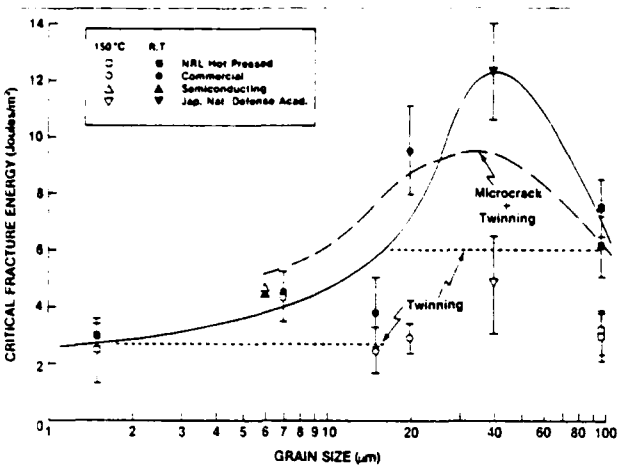

Figure 3. Critical fracture energy of barium titanate as a function of grain size at both 25°C and 150° C. Solid curve is the best fit to the 25° C data. The dashed line represents the model derived by Rice and Freiman [8]. Note that the 150° C fracture energy of all the materials is independent of grain size (after Pohanka et al [7]).

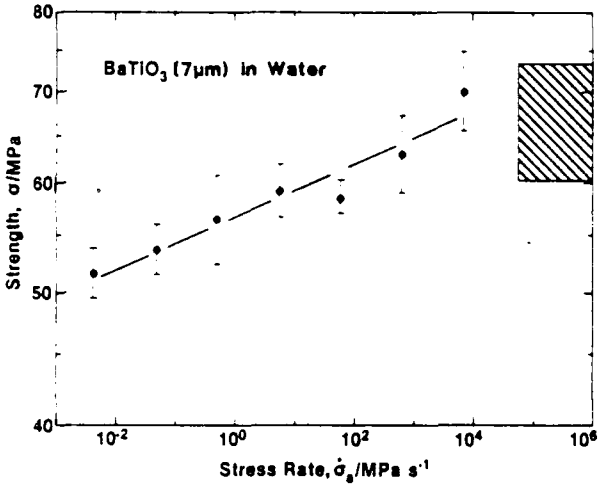

Figure 4. Stressing rate dependence of the strength of a commercial barium titanate (same material as in Figure 2) tested in water at 25° C. The material was indented with a 30N load before testing. Crosshatched area is the strength under rapid loading in inert conditions. The slope of the curve is a measure of the materials susceptibility to moisture enhanced crack growth (after Cook et al [3]).

Barium titanate, like almost all ceramics, is sensitive to moisture enhanced crack growth. The moisture enhanced fracture process can be characterized by measuring the strength of the material as a function of stressing rate as shown in Figure 4. The slope of this plot can be used to calculate a value for N, the exponent in the crack growth expression:

$$V = Vo(K_I/K_{IC})^N \qquad (1)$$

where V is the crack velocity, K_I is the stress intensity factor at the crack tip, and V_o and N are empirical constants that depend on material and environment. The data in Figure 4 yielded a value of N of 67 for this commercial barium titanate, indicating that this material is less susceptible to delayed fracture than soda lime glass for instance (N=17). Freiman et al [9] also showed that cracks in electrically poled barium titanate grew more rapidly than those in the unpoled material.

3. PZT

Unlike barium titanate, which in general can be thought of as a single compound ($BaTiO_3$), PZT occurs as a series of solid solutions of $PbZrO_3$ with $PbTiO_3$, and can exist in various crystal structures [10]. As with barium titanate, the fracture toughness of PZT is significantly higher in the ferroelectric state than in the paraelectric state for all PZT compositions [7,11], with the larger value of K_{IC} in the ferroelectric material again being of least partially due to crack-twin interactions which cannot occur above the Curie temperature.

In PZT, we can also examine the effect of changing chemistry on the fracture behavior of the material in the ferroelectric state. The room temperature fracture toughness of PZT over a range of Zr/Ti ratios is presented in Figure 5. The data appear to pass through a series of maxima and minima in K_{IC}, with a very distinct minimum

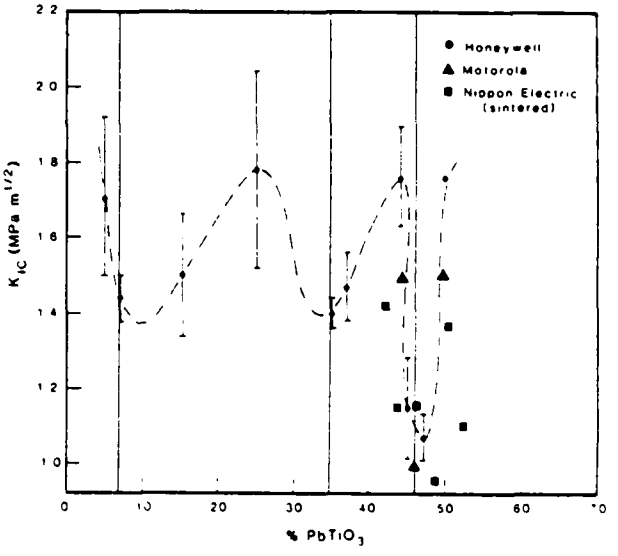

Figure 5. Critical fracture toughness, K_{IC}, of PZT as a function of the $PbTiO_3$ in the material. The vertical lines represent the positions of the phase boundaries (after Freiman et al [11]).

occurring at the morphotropic boundary between the tetragonal and rhombohedral phases. The other minima in K_{IC} also appear at phase boundaries. It was concluded by Freiman et al [11] that these minima were due to a trade-off between contributions to K_{IC} of twin crack interactions and microcracking. Because twin motion is easier at phase boundaries, the internal stresses and therefore the degree of microcracking will be minimized at these compositions, leading to minima in fracture toughness. The data in Figure 5 is similar to that obtained by Igarashi and Okazaki [12] who showed that both strength and K_{IC} are a minimum at the morphotropic boundary.

At PZT compositions near 95% $PbZrO_3$ -5% $PbTiO_3$, i.e. near the boundary between the ferroelectric, rhombohedral phase and the antiferroelectric, pnase, other interesting phenomena are observed. A primary observation is that if a 95/5 PZT specimen is electrically poled and subsequently depoled by being driven through the ferroelectric/antiferroelectric boundary by the application of hydrostatic pressure, the fracture toughness of the pressure depoled material measured at room temperature is at least 50% greater than that of either the as-fired or poled material [11]. Freiman et al [11] showed that the difference in K_{IC} between the poled and pressure depoled material decreased to zero at a temperature of approximately -65° C. These authors hypothesized that the additional toughening brought about by pressure depoling is due to the stress induced transformation of antiferroelectric domains in the vicinity of the crack tip. These domains exist in what should otherwise be a single ferroelectric phase because the pressure induced transformation from ferroelectric to antiferroelectric phases is not fully reversible [13] so that upon removal of the pressure, remnants of the antiferroelectric phase remain. The presence of residual antiferroelectric domains in the ferroelectric material has been determined both microscopically [14] and electrically [15]. Freiman et al [11] also showed through indentation-fracture measurements, that the fracture toughness of 95/5 PZT is sensitive to the lead content in the material (Figure 6). As the stoichiometry of the compound $Pb_yNb_{.02}(Zr_{.96}Ti_{.04})_{.98}O_3$ was varied from y = .96 to y = 1.02, the K_{IC} of the annealed material decreased from approximately 1.7 to 1.2. The composition having the highest K_{IC} is also the one showing the largest ratio of transgranular to intergranular fracture. Conversely, the lowest toughness material showed almost entirely intergranular fracture, implying that the excess lead is contributing to the relative weakness of the grain boundaries.

In addition, Freiman et al [11] used the indentation-fracture data to demonstrate the existence of internal stresses in this material. The magnitude of internal stress, as determined by the deviation of the data from the indentation model at small indentation loads, varied with the stoichiometry of the material. The minimum effective internal stress is observed at approximately the lead content corresponding to the stoichimetric compound. This minimum in

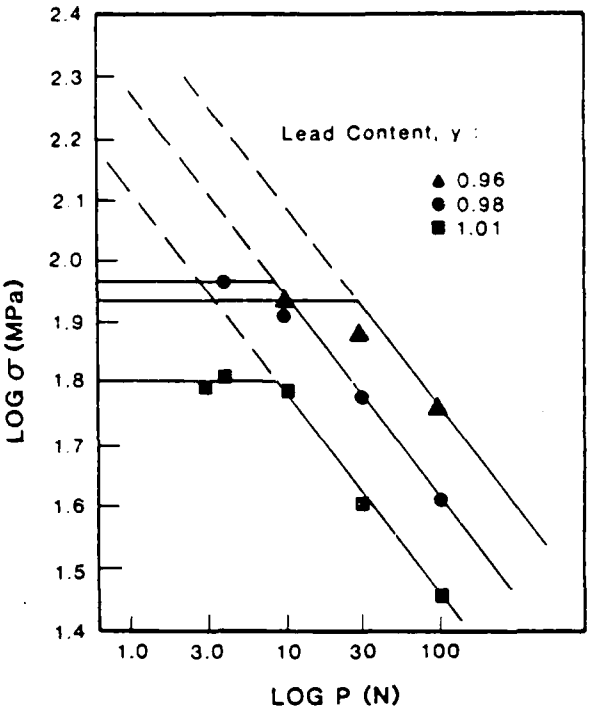

Figure 6. Indentation-fracture data for a 95/5 PZT ceramic $[Pb_yNb_{.02}(Zr_{.96}Ti_{.04})_{.98}O_3]$ in which y varied from 0.96 to 1.01. Positions of the curves of slope, -1/3, are indicative of the K_{IC} of each material. Strength plateaus are a measure of the effect of internal stresses (after Freiman et al [11]).

internal stress occurs at the same composition at which the greatest symmetry in the electrical polarization curves is observed, in agreement with the data of Dungan and Storz [16].

Like barium titanate, PZT undergoes moisture enhanced subcritical crack growth [9,17]. Direct crack growth measurements by Freiman et al [9] and Bruce et al [17] show that the rate of crack growth is dependent on the partial pressure of water in the environment and the test temperature. The slopes of the crack velocity-K_I curves determined directly, as above, are in good agreement with those obtained through stressing rate procedures [18]. Bruce et al [17] also showed that the slope and position of the crack growth curves for a PZT III ceramic were also a function of whether the material had been poled parallel or perpendicular to the crack plane. A more recent analysis of the data of Bruce et al. has suggested that the elastic anisotropy produced by the poling, rather than changes in the piezoelectric properties of the material, is the major determinant of their observed difference in crack growth [19]. Finally, McHenry and Koepke [20] showed that the application of an electric field perpendicular to the crack plane in PZT strongly affected crack propagation behavior. K_I-v curves were shifted to lower K_I's with increasing applied voltage.

As an illustration that fracture of piezoelectric ceramics can occur, not only due to purely mechanical loads, but because of the electroelastic nature of the material, we refer to the work of Ponanka et al [21]. These authors showed that driving PZT specimens at a resonant frequency could produce mechanical failure, if the applied voltage was sufficiently high. As can be seen in Figure 7, the fracture stress produced by a single tone burst is in excellent agreement with that predicted from flexural strength data. The fracture data due to multiple tone bursts also fell on this same curve. Also plotted in Figure 7, are three data points obtained by cw excitation of the PZT specimens. The stresses required to fracture the material under these conditions are smaller than would be predicted from the measured flaw size on the fracture surface. Pohanka et al suggested that a fatigue mechanism of some type must be taking place to account for the lower stress cw data.

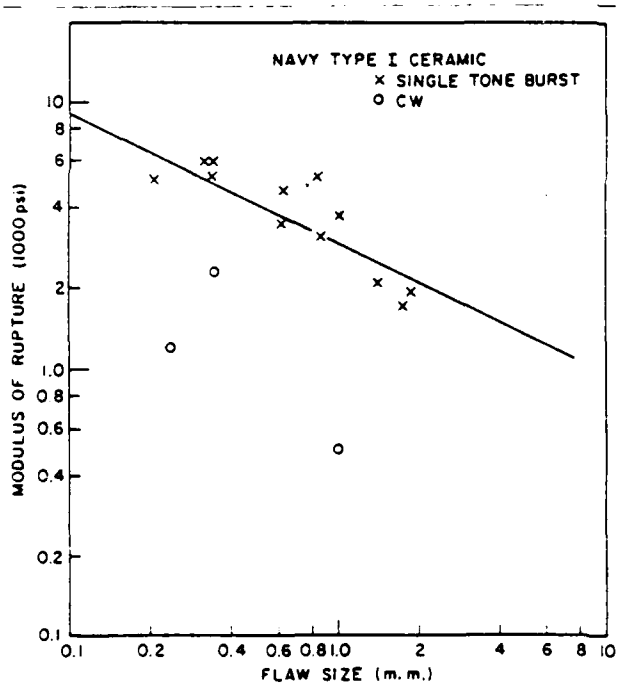

Figure 7. Fracture stress of a commercial PZT as a function of the flaw size measured on the fracture surface. Measurements were made by driving specimens at their resonant frequency either with a single pulse or with a CW signal. The curve represents the flexural strength data for the material obtained by conventional techniques (after Pohanka et al [21]).

4. Capacitor Ceramics

Multilayer ceramic capacitors are generally composed of barium titanate and related compounds whose mechanical properties can be characterized in much the same way as the materials discussed in the previous sections. Indentation-fracture techniques have been used to determine the strength, fracture toughness and subcritical crack growth behavior in a number of capacitor ceramics [22]. Values of K_{IC} for four different capacitor compositions, obtained by measuring strength under inert conditions as a function of indentation load are presented in Table 1. These values of fracture toughness are in general agreement with other data obtained on similar materials.

Table 1

Compositions and Properties of Capacitor Ceramics

Designation	Major Constituent	Grain size (μm)	K_{IC} (MPa m$^{1/2}$)	%
NPO	Rare earth oxide	1-3	1.1	44
Z5U	$BaTiO_3$	3-7	2	56
X7R	$BaTiO_3$ (+Bi)	5-1	1.1	55
X7R	$BaTiO_3$	5-1	2.7	55

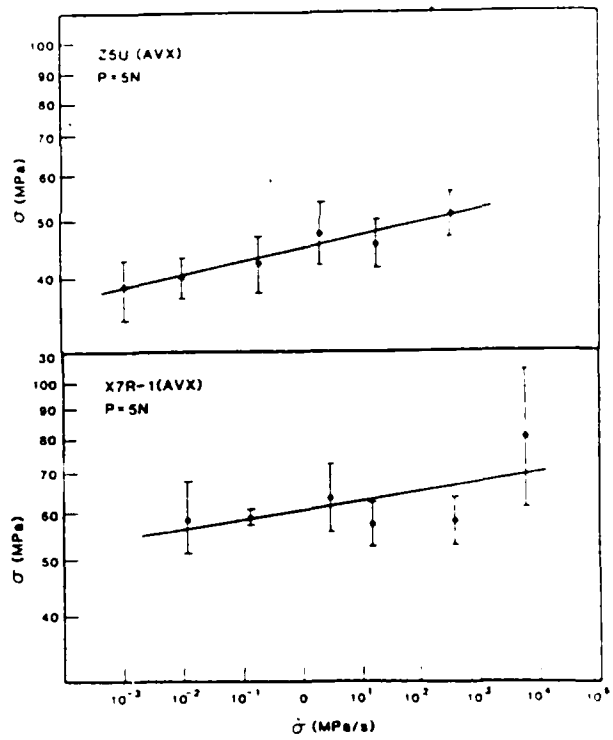

Figure 8. Stressing rate dependence of the strength of two capacitor ceramics Z5U and X7R. Data was obtained on indented squares of material in water (n = 5 specimens/data point). Note the lack of change in strength for the lower 5 stressing rates in X7R material suggesting the existence of a crack growth limit (after Baker and Freiman [22]).

Like the previous materials, capacitor ceramics also undergo slow crack growth in the presence of water. The susceptibility to moisture enhanced fracture in several of these materials has been characterized by measuring biaxial strength as a function of loading rate on indented specimens, as shown in Figure 8 [22]. The slopes of these curves can be used to calculate the exponent, N, in Equation 1. Values of N determined from best fit lines to the data in Figure 8 and given in Table 1 suggest that the susceptibility to crack growth in water can vary markedly from one capacitor composition to another probably because of differences in the chemistry of the material. There is another interesting facet to the plot for the X7R composition shown in Figure 8. If the highest stressing rate point is eliminated, the stressing rate curve is virtually flat, implying that no crack growth takes place before failure at these rates of loading. Baker and Freiman [22] suggested that the data could be explained by the existence of a crack growth limit in this material.

5. Overall Picture

Although we clearly do not have all of the answers to the problem of the mechanical failure of piezoelectric/ferroelectric ceramics, work produced over the past few years permits us make some general statements regarding this phenomenon. One of the clearest results is that while the fracture toughness of these materials in the ferroelectric state is ≥ to that in the paraelectric state, the strength follows an opposite trend. This difference in behavior is interpreted in terms of the size of the crack appropriate to strength or K_{IC} measurements. The experimental results obtained to date suggest that when the crack is small relative to the grain size in the material, i.e. $c \leq \sim 3G$, local microstructural tensile stresses generated during the paraelectric to ferroelectric phase transformation at the Curie point act as an additional driving force for fracture, thereby reducing the measured strength. At larger crack sizes, these tensile stresses are by necessity balanced by compressive stresses formed at the same time, so that throughout the whole body, the net stress is zero. The magnitude of these stresses determined by strength measurements is in excellent agreement with those predicted from dielectric theory. Preliminary data suggest that correlations can be drawn between the effect of these internal stresses on strength and the dielectric aging rate of a capacitor material [22].

The crack growth resistance of ferroelectric materials is governed by many factors, including grain size, grain boundary chemistry, and the crystal phase distribution. Contributions to fracture toughness include crack-twin interactions, crack deflection, microcracking, and possibly phase transformations at crack tips. Quantitative models involving some of these processes have been developed, but much more work is needed.

At present, no clear picture exists of the effects of an electric field on fracture. Electric fields such as would be present during the operation of dielectric or ferroelectric devices could affect fracture in a number of ways, e.g., changing the domain orientation, producing additional stresses due to piezoelectric or electrostrictive behavior, or causing elastic anisotropy. Except for the work of McHenry and Koepke [20], little work of any kind has been published on this topic.

Only a few experiments involving cyclically applied stresses have been performed [21,23]. Results of these studies suggest that phenomena other than those occuring under static loads may be responsible for the failure of piezoelectric ceramics under more complex stressing conditions. For instance, Ponanka et al [21], by analyzing the data, of Takanashi et al [23], suggested that two different mechanisms could be acting in the cyclic failure of PZT.

Environmentally enhanced crack growth occurs in all piezoelectric ceramics due to the stress aided reaction of water with the atomic bonds at the crack tip. However, there are indications from some of the data on capacitor materials that a crack growth limit may exist, below which subcritical crack extension does not take place. The susceptibility of a particular material to environmentally enhanced crack growth seems to depend strongly on its chemical composition, particularly with respect to the composition of the grain boundaries. Further knowledge of this phenomenon could help the component designer choose materials on the basis of mechanical reliability as well as their ferroelectric or dielectric properties.

6. Acknowledgements

Much of the work performed by the author has been supported by the Office of Naval Research and by Sandia National Laboratories. The many helpful discussions with Bob Ponanka are gratefully acknowledged.

References

(1) R. C. Ponanka, R. W. Rice, and B. E. Walker, Jr., "Effect of Internal Stress on the Strength of $BaTiO_3$," J. Am. Ceram. Soc., vol. 59, pp. 71-74, 1976.

(2) W. R. Buessem, L. E. Cross, and A. K. Goswami, "Phenomenological Theory of High Permittivity in Fine-Grained Barium Titanate," J. Am. Ceram. Soc., vol. 49, pp. 33-36, 1966.

(3) R. F. Cook, S. W. Freiman, B. R. Lawn, and R. C. Ponanka, "Fracture of Ferroelectric Ceramics," Ferroelectrics, vol. 50, pp. 267-272, 1983.

(4) P. Chantikul, G. R. Anstis, B. R. Lawn, and D. B. Marshall, "A Critical Evaluation of Indentation Techniques for Measuring Fracture Toughness: II, Strength Method," J. Am. Ceram. Soc., vol. 64, pp. 539-543, 1981.

(5) R. C. Ponanka, S. W. Freiman, and B. A. Bender, Effect of the Phase Transformation on the Fracture Benavior of $BaTiO_3$," J. Am. Ceram. Soc., vol. 61, pp. 72-75, 1978.
(6) G. de With and J. E. D. Parren, "Fracture of Modified $BaTiO_3$ Ceramics," Silicates Industriels, vol. 9, pp. 179-183, 1984.
(7) R. C. Ponanka, S. W. Freiman, K. Okazaki, and S. Tashiro, "Fracture of Piezoelectric Materials," in Fracture Mechanics of Ceramics, Vol. 5, ed. by R. C. Bradt, A. G. Evans, n. P. H. Hasselman, and F. F. Lange, Plenum Press, New York, 1983, pp. 353-364.
(8) R. W. Rice and S. W. Freiman, "Grain-Size Dependence of Fracture Energy in Ceramics: II, A Model for Noncubic Materials," J. Am. Ceram. Soc., vol. 64, pp. 350-354, 1981.
(9) S. W. Freiman, K. R. McKinney, and H. L. Smith, "Slow Crack Growth in Polycrystalline Ceramics," in Fracture Mechanics of Ceramics, Vol. 2, ed. by R. C. Bradt, D. P. H. Hasselman, and F. F. Lange, Plenum Press, New York, 1974, pp. 659-676.
(10) B. Jaffe, W. R. Cook, and H. Jaffe, Piezoelectric Ceramics. New York: Academic Press, 1971, p. 136.
(11) S. W. Freiman, L. Chuck, J. J. Mecholsky, D. L. Shelleman, and L. J. Storz, "Fracture Mechanisms in Lead Zirconate Titanate Ceramics," to be published in Fracture Mechanics of Ceramics, Vol. 7-8 ed. by R. C. Bradt, D. P. H. Hasselman, A. G. Evans, and F. F. Lange, Plenum Press, New York, 1986.
(12) S. Tashiro, H. Igarashi, and K. Okazaki, Jpn. J. Appl. Phys., vol. 20, Suppl. 20-4, pp. 197-203, 1981.
(13) I. J. Fritz and J. D. Keck, "Pressure-Temperature Phase Diagrams for Several Modified Lead Zirconate Ceramics," J. Phys. Chem. Solids, vol. 39, pp. 1163-1167, 1978.
(14) K. Kuroda and A. H. Heuer, in Proc. of 41st Annual Meeting of Micros. Soc. of America, San Francisco Press, San Francisco, CA, 1983.
(15) R. K. Spears, "Dielectric Characteristics of PZT 95/5 Ferroelectric Ceramics at High Pressures," Ferroelectrics, vol. 37, pp. 653-656, 1981.
(16) R. H. Dungan and L. J. Storz, "Relation between Chemical, Mechanical, and Electrical Properties of Nb_2O_5-Modified 95 Mol% $PbZrO_3$-5 Mol% $PbTiO_3$," J. Am. Ceram. Soc., vol. 68, pp. 530-533, 1985.
(17) J. G. Bruce, W. W. Gerberich, and B. G. Koepke, "Subcritical Crack Growth in PZT," in Fracture Mechanics of Ceramics, Vol. 4, ed. by R. C. Bradt, D. P. H. Hasselman, and F. F. Lange, Plenum Press, New York, 1978, pp. 687-709.
(18) R. F. Caldwell and R. C. Bradt, "Stressing Rate Effects on the Bend and Compressive Strengths of a Piezoelectric Ceramic," J. Am. Ceram. Soc., vol. 60, pp. 168-170, 1977.
(19) G. G. Pisarenko, V. M. Chushko, and S. P. Kovalev, "Anisotropy of Fracture Toughness of Piezoelectric Ceramics," J. Am. Ceram. Soc., vol. 68, pp. 259-265, 1985.
(20) K. D. McHenry and B. G. Koepke, "Electric Field Effects on Subcritical Crack Growth in PZT," in Fracture Mechanics of Ceramics, Vol. 5, ed. by R. C. Bradt, A. G. Evans, D. P. H. Hasselman, and F. F. Lange, Plenum Press, New York, 1983, pp. 337-352.
(21) R. C. Ponanka, P. L. Smith, and J. Pasternak, "The Static and Dynamic Strength of Piezoelectric Materials," Ferroelectrics, vol. 50, pp. 285-291, 1983.
(22) L. L. Baker and S. W. Freiman, "Fracture Benavior of Ceramics Used in Multilayer Capacitors," to be publisned by the Materials Research Society.
(23) S. Takahasni, E. Mori, Y. Tsuda, S. Kaneko, M. Ide, and E. Ohiro, "Fatigue Test of Magnetostrictive and Electrostrictive Materials," J. Acoustic Soc. Japan, vol. 28, pp. 241-251, 1972.

SECURITY CLASSIFICATION OF THIS PAGE (When Data Entered)

REPORT DOCUMENTATION PAGE		READ INSTRUCTIONS BEFORE COMPLETING FORM
1. REPORT NUMBER	2. GOVT ACCESSION NO.	3. RECIPIENT'S CATALOG NUMBER AD-A190501
4. TITLE (and Subtitle) Stress Corrosion of Ceramic Materials		5. TYPE OF REPORT & PERIOD COVERED Annual 1 Oct 1985- 31 Sept 1986
		6. PERFORMING ORG. REPORT NUMBER
7. AUTHOR(s) S.W. Freiman, G.S. White, T.L. Baker, S. M. Wiederhorn, T.D. Coyle, A.M. Wilson, and L. Chuck		8. CONTRACT OR GRANT NUMBER(s) N00014-86-F-0022
9. PERFORMING ORGANIZATION NAME AND ADDRESS National Bureau of Standards Ceramics Division, Rm. A329, Bldg. 223 Gaithersburg, MD 20899		10. PROGRAM ELEMENT, PROJECT, TASK AREA & WORK UNIT NUMBERS
11. CONTROLLING OFFICE NAME AND ADDRESS		12. REPORT DATE 30 Nov., 1987
		13. NUMBER OF PAGES
14. MONITORING AGENCY NAME & ADDRESS(if different from Controlling Office)		15. SECURITY CLASS. (of this report)
		15a. DECLASSIFICATION/DOWNGRADING SCHEDULE

16. DISTRIBUTION STATEMENT (of this Report)

17. DISTRIBUTION STATEMENT (of the abstract entered in Block 20, if different from Report)

18. SUPPLEMENTARY NOTES

19. KEY WORDS (Continue on reverse side if necessary and identify by block number)

Crack growth; fracture; stress corrosion; ceramics; glasses; capacitors; dielectric; gallium arsenide

Liquid ... Czochralski

20. ABSTRACT (Continue on reverse side if necessary and identify by block number)

Environmentally enhanced crack growth data was obtained on GaAs in water and methanol. No effect of NH_3 was observed. Strains in the LEC GaAs crystal were mapped using x-ray topography. Critical fracture toughness and dynamic fatigue data were obtained on capacitor ceramics of varying composition and microstructure. A wide range of values for K_{IC} and crack growth exponent, N, were observed. Collaborative work with Draper Labs and North American Phillip was performed in an effort to develop a non-destructive crack detection proced

DD FORM 1 JAN 73 1473 EDITION OF 1 NOV 65 IS OBSOLETE
S/N 0102-LF-014-6601

SECURITY CLASSIFICATION OF THIS PAGE (When Data Ente

END

DATE

FILMED

DTIC

4/88